SCIENTIFIC REPORT

NASA RESEARCH GRANT NGR-22-011-007

INTER-RELATIONS BETWEEN ADVANCED PROCESSING TECHNIQUES, INTEGRATED CIRCUITS, MATERIALS DEVELOPMENT AND ANALYSIS

by

W. B. Nowak
B. L. Cochrun
W. Carlson

Northeastern University
Boston, Massachusetts

1 January 1969

The research reported here was sponsored by the National Aeronautics and Space Administration under Research Grant NGR-22-011-007 for the period from 1 December 1967 through 30 November 1968. This report is published for information purpose only and does not represent recommendations or conclusions of the sponsoring agency. Reproduction in whole or part is permitted for any purpose of the United States Government.

RESEARCH STAFF

Welville B. Nowak, Co-principal Investigator
Professor of Mechanical Engineering

Basil L. Cochrun, Co-principal Investigator
Associate Professor of Electrical Engineering

Samuel Fine, Professor Bio-Medical Engineering

William Carlson, Engineer

T. Hull, Graduate Student

P. Salmon, Graduate Student

D. MacKeen, Graduate Student

TABLE OF CONTENTS

Section I

Active Integrated Circuits

B. L. Cochrun

I. Introduction

This section covers the investigation of simulated inductances desired for integrated circuits under NASA Grant NGR-22-011-007 from 1 December 1967 through 30 November 1968.

Attention has been given to both theoretical analysis and experimental verification of circuits suitable for integrated circuits. Active devices that have been considered include gyrators, inductance simulators, mutators, scalors and two terminal current sources. The current sources were considered as a result of attempting to increase the reliability and quality of practical gyrators.

Mr. R. W. Daniels during this past year has been preparing his doctoral thesis on active circuits as related to gyrators. The staff has participated in various seminars with Mr. Daniels. As a result, the work in the grant has profited with minimal cost to the grant in terms of expended funds.

A. Gyrators

The basic circuit of the Sipress and Witt gyrator[1], (S-W gyrator), also referred to as the Shenoi gyrator[2], is shown in Figure 1 along with the simplified model of the bipolar transistors used in the analysis and the gyrator admittance matrix. The Y matrix reflects the simplification resulting from the assumed model and thus does not include various difficulties encountered in practical gyrators.

This is a 4-port active negative feedback type gyrator. This circuit has the advantages of simplicity. In addition the collector of Q_1 is free to be used as a source of output signal and an input signal may be applied in any of several places without interferring with gyrator operation. The circuit is useful as a tuned amplifier stage when the ports are terminated

with capacitors.

Richard W. Daniels in his work at Northeastern University on his doctoral thesis has developed a synthesis procedure for active circuits which he has applied to the investigation of gyrator circuits. In particular, he has made a systematic study of several classes of gyrators and has found all the ways that they can be realized with three transistors, and in so doing has discovered a great many new gyrator configurations.

Among the gyrators that Daniels has examined is the 4-port active negative feedback type. The resistors used in making the basic gyrator circuit are considered to terminate ports of an active circuit, thus a 4-port type means that two of the ports are terminated with resistance and the remaining 2-port is the gyrator. This type is modified by the addition of a fifth port which when resistively terminated adds a negative term to either y_{11} or y_{22} (or z_{11} or z_{22} if the synthesis is based on the impedance matrix) and allows tuning out all or part of y_{11} or y_{22} according to the value of resistance terminating the added port. If either y_{11} or y_{22} can be reduced, the Q can be increased, but because of sensitivity considerations there is a limit to the improvement that is practical.

B. Gyrator Stability

It is shown in Appendix A that, based on the assumed simplified transistor model of Figure 1, the S-W gyrator is for all practical purposes potentially unstable for

$$\omega > 2\omega_{\alpha 2}\omega_{\alpha 3}/(\omega_{\alpha 2} + \omega_{\alpha 3})\ (\beta_{01}\beta_{02})^{1/2}. \qquad (1)$$

The gyrator becomes unconditionally stable again at some high frequency outside the range of its usefulness. If the transistors used in the gyrator are identical, Equation (1) shows the gyrator to be potentially unstable above the beta cutoff frequency.

The S-W gyrator is short circuit stable and may be operated stably in the region of potential instability if terminated with sufficiently large capacitive loads. One of the important uses of the gyrator is in a tuned

circuit obtained by terminating both ports with capacitors. It is of interest, therefore, to see what sort of capacitive loads are required for stable operation. An estimate of the capacitance required at one port in order that the real part of the input admittance seen at the other port be always positive was made in an earlier report.[3] Requiring the input admittance to be positive real is more restrictive than requiring the poles and zeros to be in the left half plane to insure stability; but the estimate was made in this way because it seemed easier to do. Since then another estimate has been obtained based on requiring the natural frequencies of the gyrator with capacitive loading to be in the left half plane.

Assuming that the gyrator of Figure 1 is terminated at port 1 with capacitance C_1 and at port 2 with capacitance C_2, then subject to certain assumptions some of which are given below and others mentioned in Appendix A, in which the details of the derivation are presented, the following result is obtained.

$$\tau_1\omega_{\beta 2}\omega_{\alpha 1} + \tau_2\omega_{\beta 1}\omega_{\alpha 2} > (\omega_{\alpha 1}\omega_{\alpha 2} + \omega_{\alpha 1}\omega_{\alpha 3})/\omega_{\alpha 3}; \tag{2}$$

where $\tau_1 = R_1C_1$, $\tau_2 = R_2C_2$, the number subscripts refer to the numbering of the transistors in Figure 1, and it is assumed that $\tau_1\omega_{\alpha 1} >> 1$ and $\tau_2\omega_{\alpha 2} >> 1$. If the transistors are identical, Equation (2) reduces to

$$\tau_1 + \tau_2 > 2/\omega_\beta \ . \tag{3}$$

The resonant frequency of the gyrator, terminated as described above, is

$$\omega_0 = (\tau_1\tau_2)^{-1/2} \ . \tag{4}$$

It is interesting to see that if Equation (3) is complied with the resonant frequency must be less than the beta cutoff frequency if τ_1 and τ_2 are equal. For the resonant frequency to be greater than the beta cutoff frequency τ_1 and τ_2 must be unequal.

C. Compensation for Gyrator Losses

The transistor model in Figure 1 does not include the collector-base capacitance, but it can be seen from the circuit that the collector capacitance of Q_1 appears across port 1, the collector capacitance of Q_3 is across port 2, and the collector capacitance of Q_2 couples ports 1 and 2. Thus C_1 includes the collector capacitances of Q_1 and Q_2 and C_2 includes the collector capacitances of Q_2 and Q_3. The effects of coupling between the ports are discussed in reference 3. If the magnitudes of y_{12} and y_{21} of the gyrator are unequal, the capactive coupling between ports may introduce losses or increase the possibility of instability, depending upon the loads at the ports and the nature of y_{12} and y_{21}. If y_{12} and y_{21} differ only in sign, the principal effect of the collector capacitance of Q_2 coupling the ports is to add its value to any capacitance connected to the two ports. In the ideal gyrator the y_{11} and y_{22} terms in the admittance matrix are zero. In the practical gyrator, at low frequencies where transistor phase shifts are negligible and the elements of the admittance matrix are real, the imperfect nature of bias sources and the finite gain of transistors causes y_{11} and y_{22} to be nonzero and positive for the kind of gyrators under consideration here. That is, the practical uncompensated gyrator is equivalent to an ideal gyrator loaded at each end with corresponding shunt conductance y_{11} or y_{22}. Since the maximum Q of a tuned circuit formed by terminating each port of the gyrator with capacitors is proportional to the square root of the ratio of the product of the gyration conductances divided by the product of the input conductances, it is seen that y_{11} and y_{22} set a limit on the maximum Q that can be obtained with the gyrator.

The S-W gyrator as modified by Daniels is shown in Figure 2. The added conductance G_3 appears as a negative term in y_{22}. Thus, if G_3 is chosen equal to the positive terms in y_{22}, y_{22} can be made zero and infinite Q obtained using the gyrator as a resonator, but an adjustment of this sort would be impossibly delicate. It would be practical to diminish y_{22} sufficiently to increase the Q several fold over what it would be without G_3.

A further modification of the Witt and Sipress gyrator is shown in Figure 3. This is an extension of the idea in Daniels' modification in Figure 2 to make it possible to tune both y_{11} and y_{22} to zero or to suitably reduce them. This modification did not come out of Daniels' synthesis because the circuit is a six-port (in the sense described above) and Daniels limited his investigation to modifying a four-port by adding a port to tune out one of the input admittances. Had he attempted an extension to the six-port, Figure 3 would have been one of the possible circuits. Figure 3 is a reflexed circuit, i.e., all three transistors function together as a gyrator and in pairs as negative immittance converters. With port 2 shorted, transistors Q_1 and Q_2 convert G_4 to a negative conductance at port 2. The modified circuits should be useful in making high Q circuits because, given reasonably good current sources for biasing (G_{B1} and G_{B2} small), the unmodified circuit (Figure 1) has a moderate maximum Q of roughly one-half the geometric mean of the common-emitter current gain of transistors Q_1 and Q_2 and, as Gensel[4] has observed, a Q enhancement of 10 to 20 might reasonably be accomplished (by reducing y_{11} or y_{22} or both) without the circuit becoming excessively sensitive to parameter variations.

D. Practical S-W Gyrators

The Sipress and Witt gyrator is the simplest of gyrators, its basic circuit containing three transistors and two resistors. Because one of the transistors is used as an emitter follower, its collector is available to provide an isolated output, and because it is possible to apply an input signal in a number of ways[3] without interferring with gyrator operation, it is possible to use the S-W gyrator as a tuned amplifier. If the transistors used are alike, the maximum Q of the S-W gyrator used as a resonant circuit is equal to one half of beta.

With complementary transistors the S-W gyrator may be made in direct-coupled form biased with two current sources, each being realized with a transistor.[3,5] Because it is at present difficult to make integrated circuits containing complementary transistors an effort has been made to realize the circuit in direct coupled form using only transistors of the

same polarity type. Two circuits have been discovered, one containing bipolar transistors and using field effect transistors for current sources and one containing only bipolar transistors.

The first of the new gyrator circuits is shown in Figure 4. The three bipolar transistors of the same polarity type form the basic gyrator structure (see Figure 1) and the three FET's are used as current sources in biasing. If R_1 and R_2 are equal, the gyrator is passive from the point of view of the two ports to which C_1 and C_2 are connected. This would be the usual design because coupling between ports such as through the collector-base capacitance of Q_2 does not cause regenerative or degenerative feedback as happens if R_1 and R_2 are unequal. FET current source I_1 supplies the collector current bias for Q_1, I_2 does the same for Q_3, and the collector current for Q_1 is the difference between I_3 and I_2. The FET current sources have resistors in series with the source terminals because I_{dss} was higher than the currents desired. In integrated circuit form the FET's could be designed for the currents needed but the source resistors might still be desirable because of the degenerative feedback they provide. With R_1 and R_2 equal, the collector-emitter bias voltage of Q_2 is $R_1(I_3 - I_1 - I_2)$, and I_3 must be greater than the sum of sources I_1 and I_2.

The FET's in Figure 4 are p-channel types but they could just as well be n-channel types turned end for end. The FET supplying current I_3 could be replaced with a resistor with little effect upon the operation of the circuit provided the resistance was very much greater than the resistance seen looking into the emitter of Q_3.

The input signal is shown applied to the emitter of Q_3. It could have been applied to the gate of the I_3 current source FET (returning the gate to +6v through a resistor) for higher gain. The maximum Q for this gyrator is half the square root of the product of the beta's of Q_1 and Q_2. At 168 kHz (910 pf tuning capacitors) the Q was about 33. With 68 pf capacitors the resonant frequency was 1.78 mHz with a slightly higher Q than at 168 kHz. The circuit was stable without external capacitors because of the capacitive loading provided by the collector capacitances of the transistors, current sources, and wiring (as explained in section I(b)). Without external

capacitance, the resonant frequency was 6 mHz which corresponds to about 25 pf of internal capacitance at each port.

The other new circuit is shown in Figure 5. The arrangement of transistors Q_1, Q_2 and Q_3 which make up the basic gyrator is the same as in Figure 4. Transistors Q_4, Q_5 and Q_6 serve as current sources as did the FET's in Figure 5. Q_6 is used in the ordinary way as a constant current source and needs no explanation. Q_4 in a feedback arrangement with Q_1 supplies a constant current to Q_2. There is a constant voltage $V_{Z1} - V_{BE1} - V_{BE4}$ across bias resistor R_{B1}, as can be seen by inspection of Figure 5, which sets the level of the bias current. Q_5 operates the same way together with Q_2 to supply a constant current to Q_3. Current sources Q_4 and Q_5 are not perfect and, therefore, add losses to the circuit. Current source Q_4 in effect shunts port 1 with a resistance of approximately $R_{B1}R_1(\beta_1 + 1)/[r_{e1}(\beta_1 + 1) + r_{b1}]$. Current source Q_5 similarly loads port 2. With C_1 and C_2 both 910 pf, a Q of 14 was measured at 171 kHz. The Q figure cannot be compared with that measured in the circuit of Figure 4 in order to judge which is the better circuit because different types of transistors were used, but it is likely that FET's make better current sources.

II. Inductance Simulators

Inductance can be simulated with a gyrator and a capacitor. It can also be simulated with circuits that are related to the gyrator but are simpler and are here called inductance simulators to distinguish them from gyrators. Regarded as two-port networks (with one port being located where a capacitor used in the simulation appears) the admittance matrix is similar to that of a gyrator (or PII) except that either y_{11} or y_{22} is larger where in a gyrator these are both small.

Figures 6 and 7 show the basic circuits of two inductance simulators. The equivalent circuits of y_{in} are based on the transistor model of Figure 1 at low frequencies with the addition of emitter resistance r_e to transistor Q_1 in Figure 6 because of its importance in the circuit as described in reference (3). Both circuits are simple, easily biased, and may be constructed with transistors of the same polarity type. Simulator

B is slightly more complicated than A, but for a given set of transistors has a higher Q.

Inductance simulator A as constructed with an RCA CA 3018 integrated circuit is shown in Figure 8. The CA 3018 integrated circuit contains four transistors--two independent and two with an internal connection from the emitter of one to the base of the other. If the equivalent alpha's of the compound transistors Q_1 and Q_2 were unity, the maximum Q for the circuit would be only about 4.5, assuming a Q_{1b} emitter current of about 1 milliampere and r_{e1} of 25 ohms. Circuit performance could be improved by replacing R_E with a current source and using the two transistors that make up the equivalent transistor Q_1 in a feedback circuit to form another equivalent transistor Q_1 having a much smaller effective r_{e1} (and a smaller current gain). The circuit was operated at about 20 kHz and the Q observed to be low.

Inductance simulator B was also built using the CA 3018 integrated circuit as shown in Figure 9. Here transistors Q_{1a} and Q_{1b} are connected to yield a high equivalent β_1 and the reverse biased emitter-base junction of Q_3 is used for the zener diode shown in Figure 7. A 150 kilohm resistor connected to a high voltage supply was used for a current source. A field effect transistor used as shown in Figure 4 would be more suitable in a practical application. Q_3 was a noisy zener when carrying the small current required at the base of Q_{1a}, which accounts for the 0.01 mfd by-pass capactor. The capacitor could be eliminated by placing a current sink at the base of Q_{1a} to increase the current carried by Q_3. The 22k resistor connected to the emitter of Q_{1a} is not an important part of the circuit. It increases the current carried by Q_{1a} and, in retrospect, if it were to be part of the circuit it would be more effective placed across the emitter-base terminals of Q_{1b}.

With C_1=15,000 pf and C_2=1,000 pf, a Q of 9.6 was measured at 54 kHz, which neglecting the loading effect of the 150k current source, corresponds to a beta of about 500 for the compound transistor Q_1. If the alpha of Q_1 were to be unity, the Q of the simulator would become equal to the square root of the ratio of the time constants R_1C_1 and R_2C_2 which for the circuit

shown and the values used for C_1 and C_2 is about 16. This compared to the observed Q of 9.6 shows the effects of the limited current gain of Q_1 and the losses introduced by the 150k current source.

The two inductance simulators have the merit of having simple circuits which should be realizable in integrated circuit form. Simulator A, Figure 6, is practical form is a low Q circuit. Simulator B, Figure 7, is a higher Q circuit, and if three transistors are used in its construction, as in Figure 9, the maximum Q attainable is essentially the same as for the S-W gyrator, Figure 1, which also used three transistors, but with an important difference. To obtain high Q with the simulator it is necessary that R_1C_1 be very much greater than R_2C_2 whereas with the gyrator the corresponding quantities can be of similar size in a high Q circuit, which is usually an advantage.

III. Realization of Mutators and Scalors

Chua[6] has recently described, among other things, a couple of linear two-port that are related to gyrators and active transformers. One of these he calls a mutator. It is an active linear two-port that transforms one type of nonlinear element into another. Chua considers three classes of mutators, L-R, C-R and L-C. Each class of mutator comes in two types which Chua has called types 1 and 2 but which may also be classified as noninverting or inverting according to whether the impedance seen at the input port is directly or inversely proportional to an impedance terminating the output port. The other two-port has been named scalor. It is identical to a positive immittance converter.

The L-R mutator has the property that the voltage-current curve of a nonlinear resistor connected to the output port is seen at the input port as flux-linkage versus current curve of the same shape in the noninverting type or as current versus flux-linkage curve in the case of the inverting type. Similarly, the C-R mutator generates a nonlinear capacitor at the input port when the output is terminated with a nonlinear resistor, with the charge versus voltage characteristic being identical to the voltage-current characteristic of the nonlinear resistor for the noninverting type

and to the current-voltage characteristic for the inverting type. In the same way, the L-C mutator generates at the input a nonlinear inductor having a flux-linkage versus current curve having the same shape as the charge versus voltage curve of the nonlinear capacitor connected to the output port in the noninverting type or of the shape of voltage versus charge curve in the inverting type. The inverting L-C mutator is a gyrator. The noninverting L-C mutator may be regarded as an active transformer with an imaginary turns ratio.

There are three kinds of scalors. One is the current scalor in which the ratio of the currents in the input and output ports is a real constant and the voltage ratio is unity. Another is the voltage scalor in which the voltage ratios between the two ports is a real constant and the current ratio is unity. A third is the power scalor having both current and voltage ratios real constants other than unity. The scalors are positive immittance converters (PIC) or active transformers. Table 1 lists the transmission matrices of the various mutators and scalors.

Chua shows how these two-ports and other types described in his paper can be used to synthesize nonlinear networks. He gives a number of idealized and practical realizations of mutators and scalors.

To one familiar with gyrator circuits of the active negative feedback type (as distinguished from those built around negative resistance circuits) mutators and scalors are not new concepts, although not known by these names. These circuits are in varying degrees part of the gyrator circuit. The active negative feedback type of gyrator contains within the same circuit configuration two gyrators and two or more PIC's (or active transformers). All of Chua's mutators and scalors can be realized with one three-transistor 6-port circuit, shown in Figure 10, by terminating 4 of the ports in resistors or capacitors.

Table 2 shows how all of the mutators can be realized with the circuit shown in Figure 10. It tells which ports are to be terminated with resistors, which are to be terminated with capacitors and which port is to be the output port with the input port being in all cases port 1. The terminations are given as 1 ohm resistors and 1 farad capacitors for convenience.

These are not, of course, practical values and would not be used in constructing the circuit. Table 2 gives one set of mutators, but each can be realized in another way in the circuit. Another set of mutators realizations can be obtained by replacing ports 1, 2 and 3 with ports 4, 5 and 6 and vice versa in the table. The transistor configuration is a familiar one. The gyrator seen between ports 4 and 6 when the other ports are terminated with resistors is the New and Newcomb[7] gyrator.

The three transistor circuit contains three different PIC possibilities which lead to two ways to realize each of the voltage and current scalors and one way to realize the power scalor. One of the ways of realizing the voltage and current scalors comes from making the current or voltage ratio in the power scalor unity.

The current scalor can be obtained between ports 2 and 5 with the other ports terminated with resistors to give

$$K_I = \frac{R_1 R_3}{R_4 R_6}, \quad K_V = 1, \tag{5}$$

where the subscripts correspond to the port numbers. The voltage scalor can be realized between ports 1 and 5 to give

$$K_I = 1, \text{ and } K_V = \frac{R_4 R_6}{R_2 R_3}. \tag{6}$$

And finally a power scalor can be realized between ports 2 and 4 to give

$$K_I = \frac{R_3}{R_6}, \text{ and } K_V = \frac{R_5}{R_1}. \tag{7}$$

R. W. Daniels, Bell Telephone Laboratories, North Andover and A. W. Carlson have worked together on the material presented in this section and have prepared a letter on the subject for publication.

IV. Two-Terminal Current Source

High quality gyrators usually require current sources for biasing. There are a number of ways of simulating current sources, but there are

difficulties if the gyrator proper and the biasing current sources are to use bipolar transistors of the same polarity type. Although one way, reported earlier, has been found for making particular kinds of gyrators with transistors of the same polarity type in which certain of the transistors in the gyrator are used in a feedback arrangement with additional transistors to simulate current source biasing, other better and more flexible methods have been continually sought.

A two-terminal transistor circuit for simulating a current source has been developed. The advantage of a two-terminal current source is that it can be placed anywhere in a circuit where the voltage falls within its operating range. Single bipolar transistors can serve as current sources, as is well known, the collector being a high impedance source of constant current when the emitter current is held constant, but the location of current sources of this type within a circuit is restricted and frequently, as in biasing gyrators with this method, transistors of both polarity types are needed. Depletion type field effect transistors may be used as two-terminal current sources in the same way as the circuit under consideration here.

The circuit of the two-terminal current source is shown in Figure 11 and the V-I characteristic in Figure 12. Referring to these Figures, the operation of the circuit may be explained in the following way. Suppose V to be increased starting from zero and I observed (the V-I curve traced, that is). At V equal to zero both transistors and diodes are cutoff and I is very small. This condition holds until V is large enough to forward bias the base-emitter junction of Q_2, about 0.65v for silicon transistors. With Q_2 active and Q_1 still cutoff the circuit presents a low impedance at the terminals and I increases rapidly with voltage until the current is large enough to develop a voltage across R_1 great enough to forward bias the base-emitter junction of Q_1 and increase the impedance seen at the terminals. A further increase in V brings the diodes into conduction and the circuit enters the constant current region. The function of the diodes is to provide a fairly constant current to the collector of Q_1. This current is equal to R_2 divided by the difference in potential between the

two diodes and the base-emitter voltage of Q_2. This assumes that the base current of Q_2 is small and most of this current is carried by Q_1. The current in the constant current region has as its principal component a quantity equal to the voltage drop across the base-emitter of Q_1 divided by R_1, plus the smaller, practically constant, emitter current of Q_1. The current is nearly constant because the base-emitter voltage of Q_1 is nearly constant and the base-emitter voltage is nearly constant because the collector current is nearly constant. The current is carried by Q_2 and R_3 with the proportion carried by each being dependent upon V and controlled by Q_1 acting upon the base current of Q_2. When V becomes large enough for R_3 to carry all the current, Q_2 becomes cutoff and the impedance seen at the terminals is reduced to R_3. The high impedance region is the useful part of the V-I characteristics.

In the region where both transistors are active and the diodes are forward biased, the current is substantially constant at

$$I_S \approx V_{BE1}/R_1 + (2V_D - V_{BE2})/R_2, \tag{8}$$

or about V_{BE1}/R_1 since the second component is much smaller typically. The resistance of the current source in the active region, the reciprocal of the slope of the active region in Figure 12 is approximately

$$R_S \approx \frac{R_1 R_2 R_3}{(R_1 + r_{e1})\,[2r_d + r_{e2} + R_2(1 - \alpha_2)]}, \tag{9}$$

where r_e and r_d are emitter and diode resistances (both current dependent) and the subscripts identify the transistors. Equation (9) represents the dominant term in the expression of the active region resistance and was derived using the low frequency T-equivalent circuit for the transistors under the assumption that the base resistance and the collector conductance can be neglected and that the common-emitter current gain is much greater than unity. It is sufficiently accurate for the intended use of the circuit and the values of resistance appropriate to that use. In the region where

Q_1 is off and Q_2 is active, the resistance is low and is

$$R_1 + (1 - \alpha_2)(R_2 + R_3). \tag{10}$$

The transition between the low resistance region and the high resistance constant current region is completed when both transistors are active and diodes D_1 and D_2 are forward biased. These conditions set a lower limit to the voltage in the constant current region

$$V_{min} \approx 2V_D(1 + R_3/R_2) - V_{BE2}R_3/R_2 + V_{BE1}. \tag{11}$$

At some higher voltage Q_2 becomes cutoff and all the current is carried by R_3. This voltage is the upper limit of the constant current region and is given by

$$V_{max} \approx V_{BE1}R_3/R_2 + (2V_D - V_{BE2})\ R_3/R_2 + V_{BE1} + 2V_D. \tag{12}$$

The circuit constructed, using type 2N3250 transistors, the emitter-base junctions of 2N706 transistors for the two diodes and resistance values of 470 ohms for R_1 and 10 kilohms for both R_2 and R_3 was characterized by the following measurements taken from a display of the V-I curve on an oscilloscope: $V_{min} \approx$ 2.5v., $V_{max} \approx$ 17v., the resistance in the region where Q_1 is off and Q_2 active is approximately 900 ohms. The resistance of the active region about 160 kilohms, with about 1.5 milliamperes of current in the constant current region. These values are consistent with a Q_2 beta of 50 and forward bias voltage drops of 0.65 volts on the diodes and transistor base-emitter junctions. With lower gain 2N706's in the circuit, the resistance in the active region was about 100 kilohms, corresponding to a Q_2 beta of 20, typical of this type of transistor.

The importance of this circuit is that it makes possible an integrated gyrator containing bipolar transistors of the same polarity type.

V. Projections

Consideration has been given to both the theoretical and practical aspects of inductance simulators so important to integrated circuits. Attention in the future will be given to practical application utilizing these results.

It should be possible to construct a complete tuner including the IF amplifier stage or stages using simulated inductances. The results of this study indicate that the structure should be adaptable to integrated circuit techniques. A preliminary stage will involve an integrable 455 kHz IF amplifier with a bandwidth of 10 kHz. In terms of Q this does not appear to be an unduly rigorous requirement of the circuit.

Some preliminary work has been done on the use of simulated inductances in conjunction with a varactor type amplifier. This is a d-c amplifier with high input impedance and drift characteristics similar to chopper stabilized amplifiers. The tuned circuits are required for modulation and demodulation purposes. A preliminary version has indicated the feasibility of this approach. An integrable amplifier of this type would find wide use in bio-medical applications since aside from its small size it should provide greater stability and reliability than that obtainable with discrete counterparts.

VI. REFERENCES

1. J. M. Sipress, F. S. Witt, U. S. Patent No. 3,001, 157, 19 September 1961.

2. B. A. Shenoi, "Practical Realization of a Gyrator Circuit and RC-Gyrator Filters," IEEE Transactions on Circuit Theory, Vol. CT-12, No. 3, September 1965, pp. 374-380.

3. R. E. Bach, Jr., A. W. Carlson, G. F. Currin, P. Honsinger, and P. A. Olendzenski, "Reliable Solid-State Circuits," Semiannual Report No. 6, NASA NGR-22-011-007, Northeastern University, Boston, Massachusetts, January 1, 1968.

4. J. Gensel, "Notes on the Structure of Gyrator Circuits," Proc. IEEE (Letters), Vol. 55, No. 10, October 1967, pp. 1735-1736.

5. R. E. Bach, Jr., A. W. Carlson, G. F. Currin, and R. E. Scott, Jr., "Reliable Solid-State Circuits," Semiannual Report No. 5, NASA NGR-22-011-007, Northeastern University, Boston, Massachusetts, July 1, 1967.

6. Leon O. Chua, "Synthesis of New Nonlinear Network Elements," Proc. IEEE, Vol. 56, No. 8, August 1968, pp. 1325-1340.

7. R. W. New W. Newcomb, "An Integrable Time-Variable Gyrator," Proc. IEEE, (Correspondence), Vol. 53, No. 12, December 1965, pp. 2161-2162.

8. Louis Weinberg, Network Analysis and Synthesis, McGraw-Hill Book Company, Inc., New York, 1962, pp. 237-240.

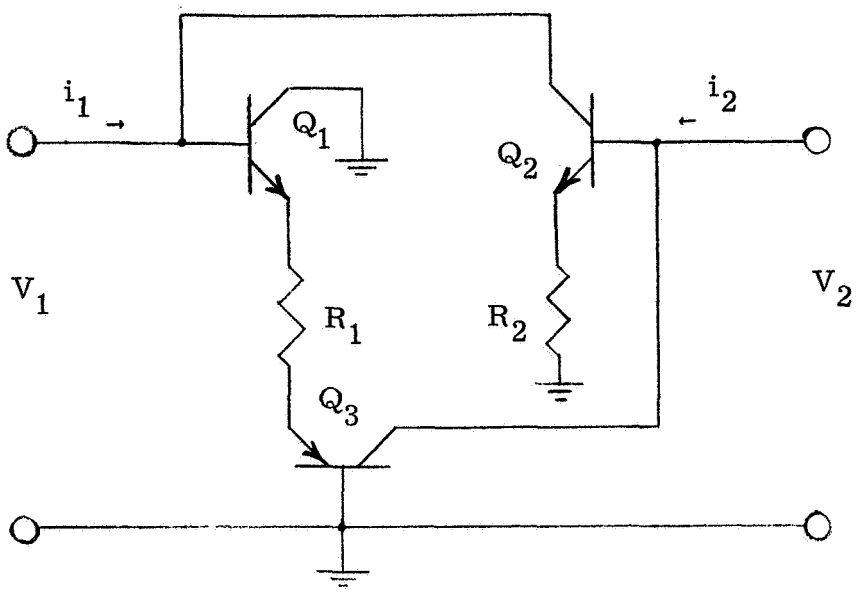

a) Basic Circuit

$$y = \begin{bmatrix} \frac{1}{R_1(\beta_1 + 1)} & \frac{\alpha_2}{R_2} \\ -\frac{\alpha_3}{R_1} & \frac{1}{R_2(\beta_2 + 1)} \end{bmatrix}$$

b) Addmittance Matrix

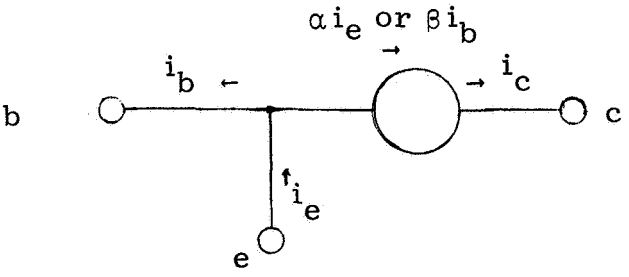

$$\alpha = \frac{\alpha_0}{1 + s/\omega_\alpha}$$

$$\beta = \frac{\beta_0}{1 + s/\omega_\beta}$$

$$\omega_\beta = (1-\alpha_0)\,\omega_\alpha$$

c) Transistor Model

Figure 1. Sipress and Witt Gyrator

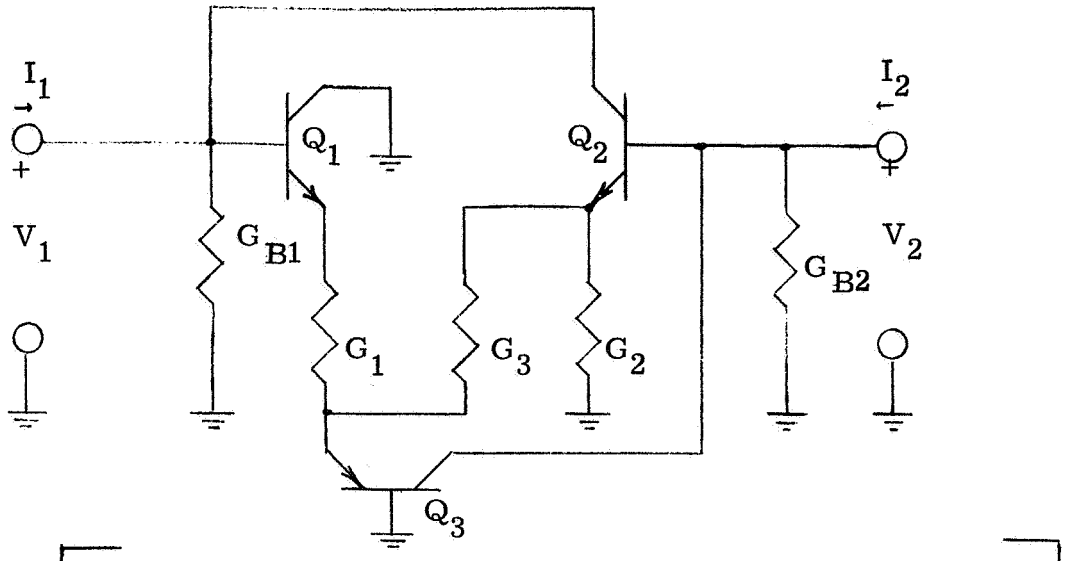

$$y \approx \begin{bmatrix} (1-\alpha_1)\,G_1 + G_{B1} & \alpha_2\,(G_2 + G_3) \\ -\alpha_3 G_1 & (1-\alpha_2)\,(G_2 + G_3) + G_{B2} - G_3 \end{bmatrix}$$

Figure 2. S-W Gyrator as Modified by Daniels

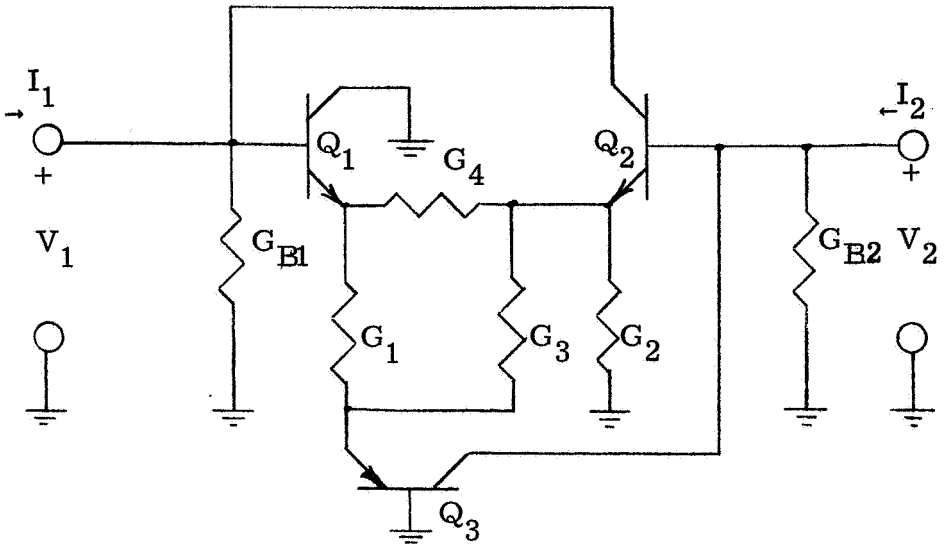

$$y \approx \begin{bmatrix} [(1-\alpha_1)(G_1 + G_4) + G_{B1} - G_4] & \alpha_2(G_2 + G_3 + G_4) \\ -\alpha_3 G_1 & [(1-\alpha_2)(G_2+G_3+G_4) + G_{B2} - G_3] \end{bmatrix}$$

Figure 3. A Further Modification of S-W Gyrator

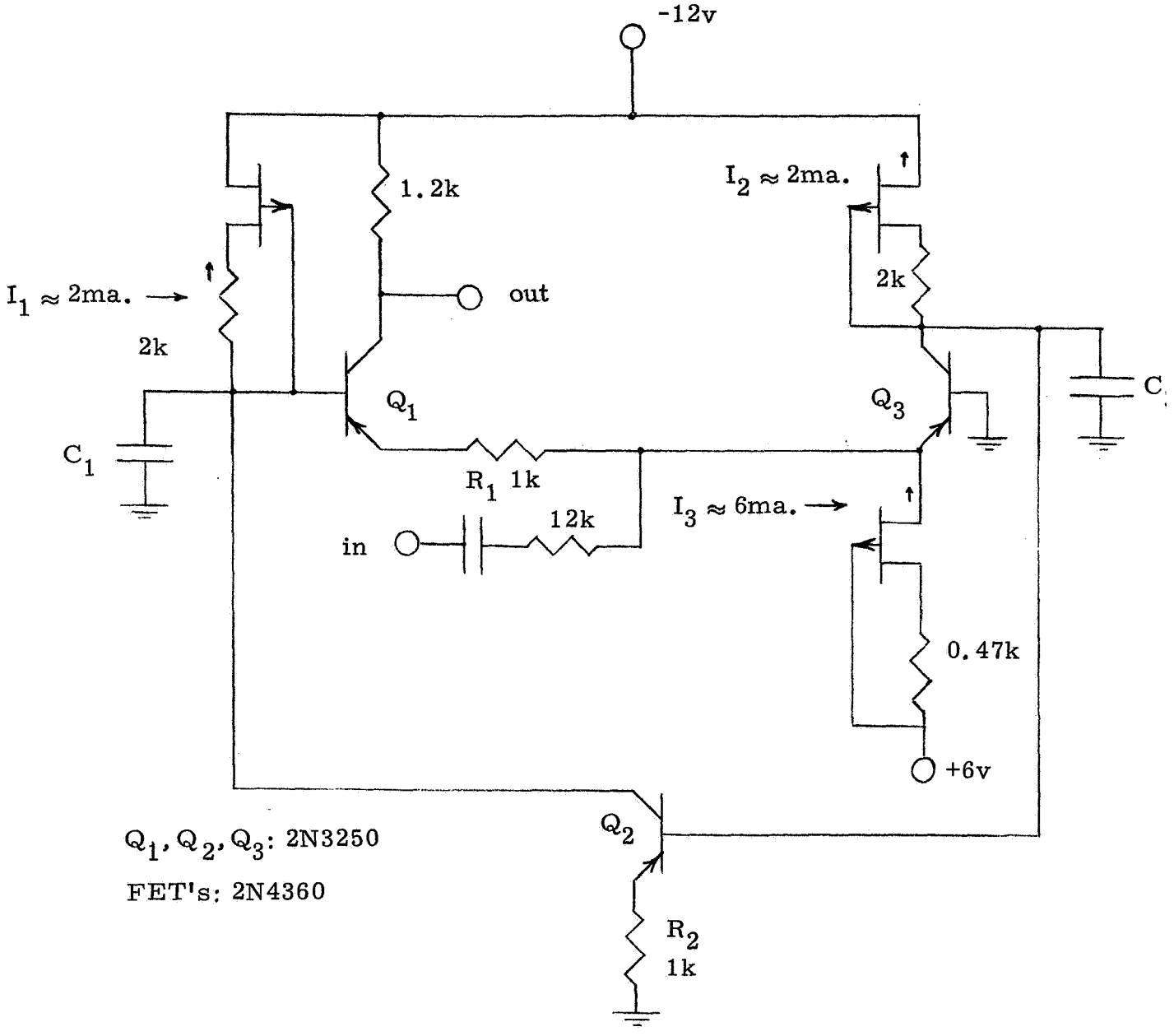

Figure 4. S-W Gyrator Made with FET and Bipolar Transistors

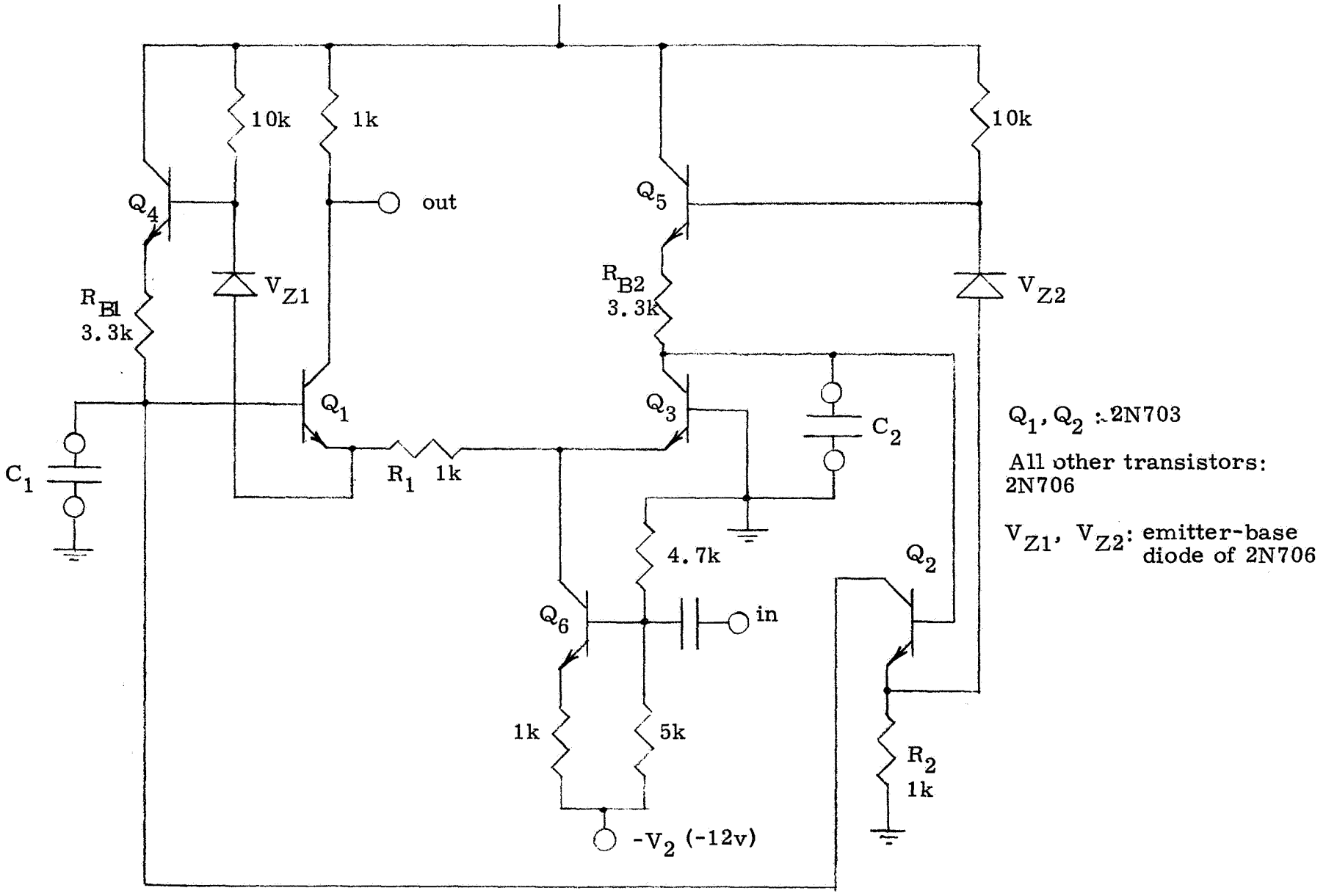

Figure 5. S-W Gyrator Made with Bipolar Transistors of the Same Polarity Type

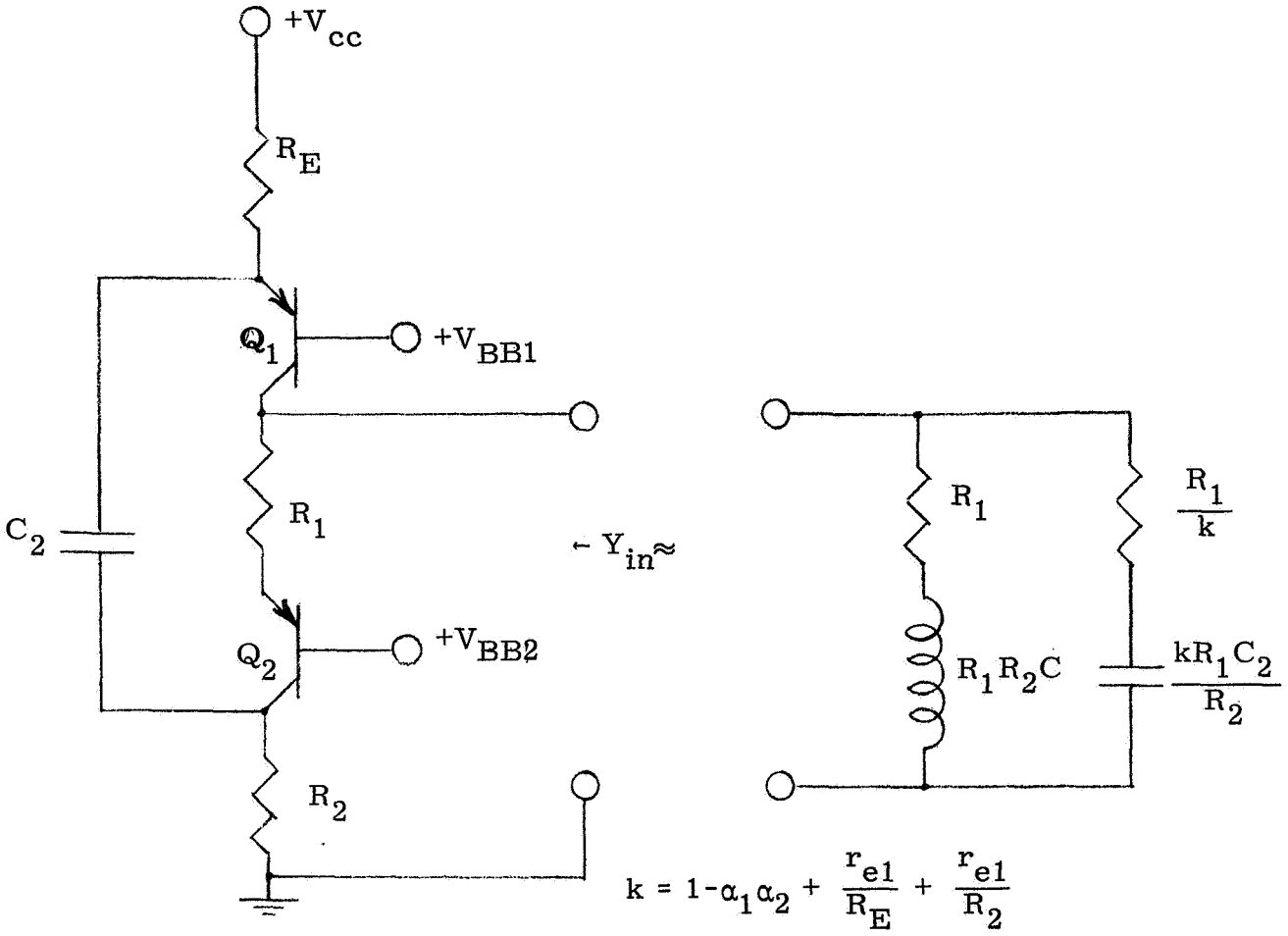

When tuned with a capacitor C_1

$$\omega_0 \approx \frac{1}{\sqrt{R_1 R_2 C_1 C_2}}$$

$$Q \approx \frac{\sqrt{R_1 R_2 C_1 C_2}}{R_1 C_1 + (1 + \frac{r_{e1}}{R_E} + \frac{r_{e1}}{R_2} - \alpha_1 \alpha_2) R_2 C_2}$$

$$Q_{max} = \frac{1}{2} \sqrt{\frac{1}{1 - \alpha_1 \alpha_2 + \frac{r_{e1}}{R_E} + \frac{r_{e1}}{R_2}}}$$

Figure 6. Inductance Simulator A

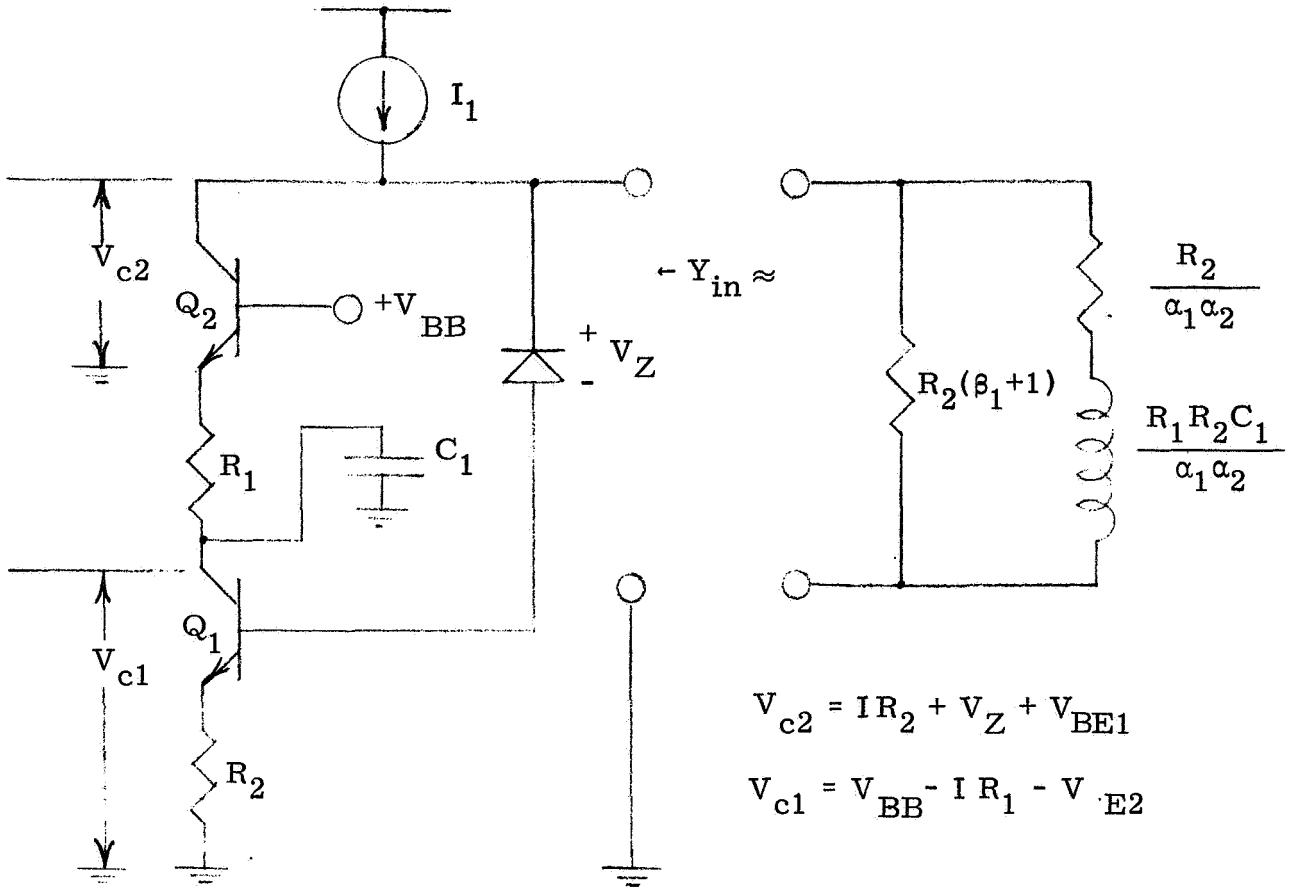

When tuned with a capacitor C_2,

$$\omega_0 \approx \frac{1}{\sqrt{R_1R_2C_1C_2}} \qquad Q \approx \frac{\sqrt{\alpha_1\alpha_2}\ \sqrt{R_1R_2C_1C_2}}{R_1C_1(1-\alpha_1) + R_2C_2}$$

Q is maximum when $R_2C_2 = R_1C_1(1-\alpha_1)$

$$Q_{max} = \frac{1}{2}\ \alpha_2^{\frac{1}{2}}\ \beta_1^{\frac{1}{2}}$$

Figure 7. Inductance Simulator B

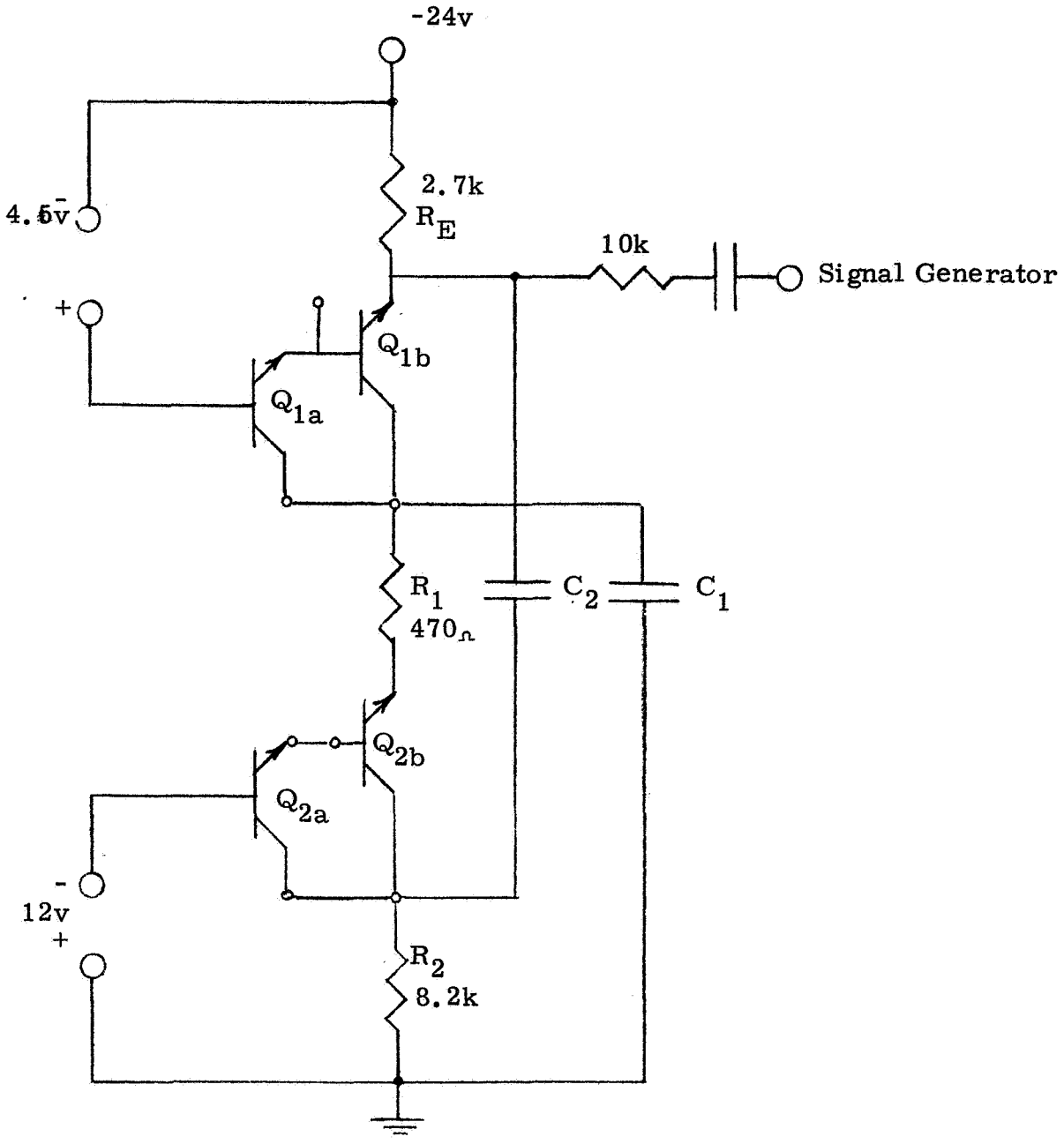

Figure 8. Inductance Simulator A as constructed Using RCA CA3018 Integrated Circuit

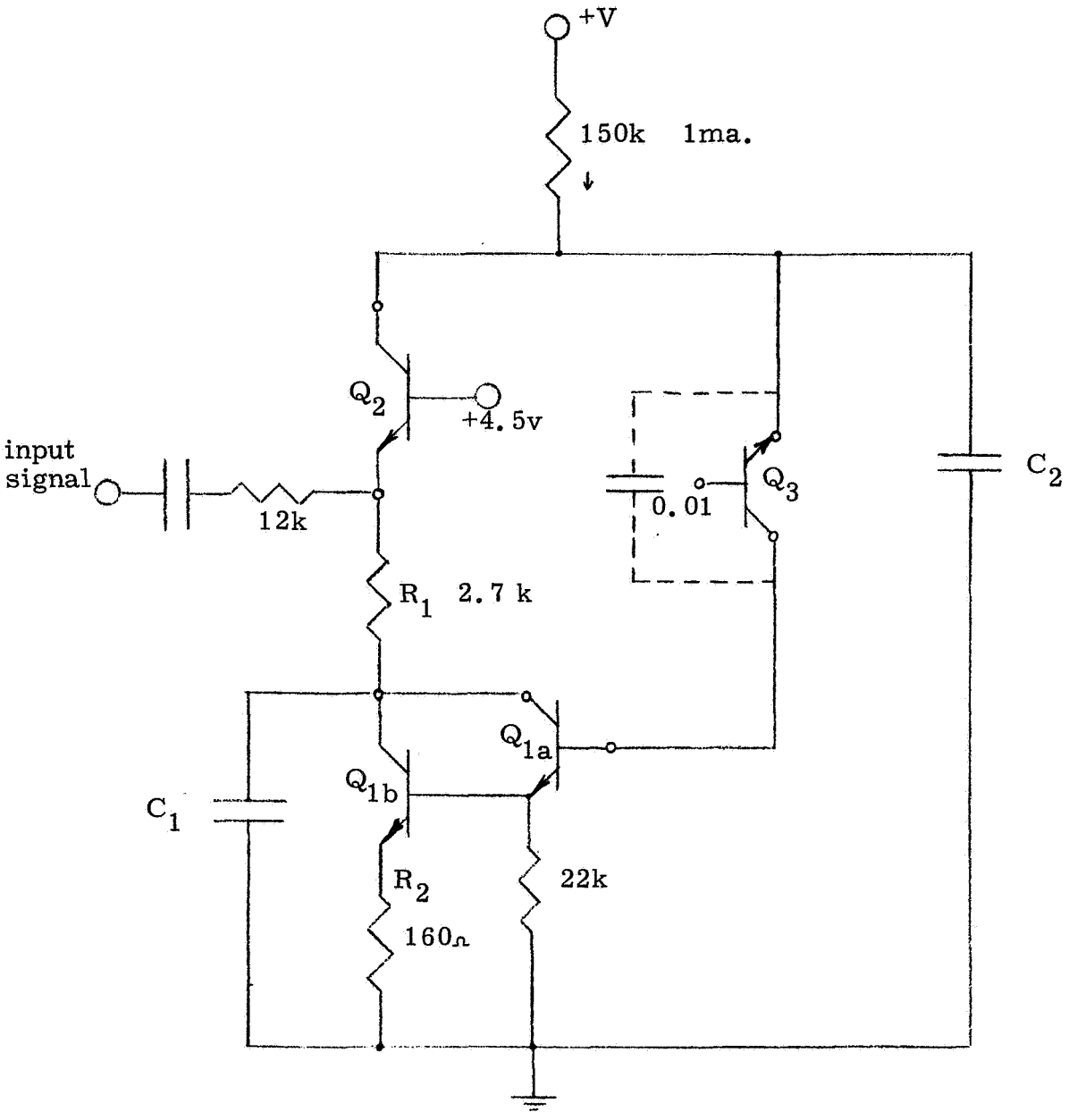

Figure 9. Inductance Simulator B as Constructed Using RCA CA3018 Integrated Circuit

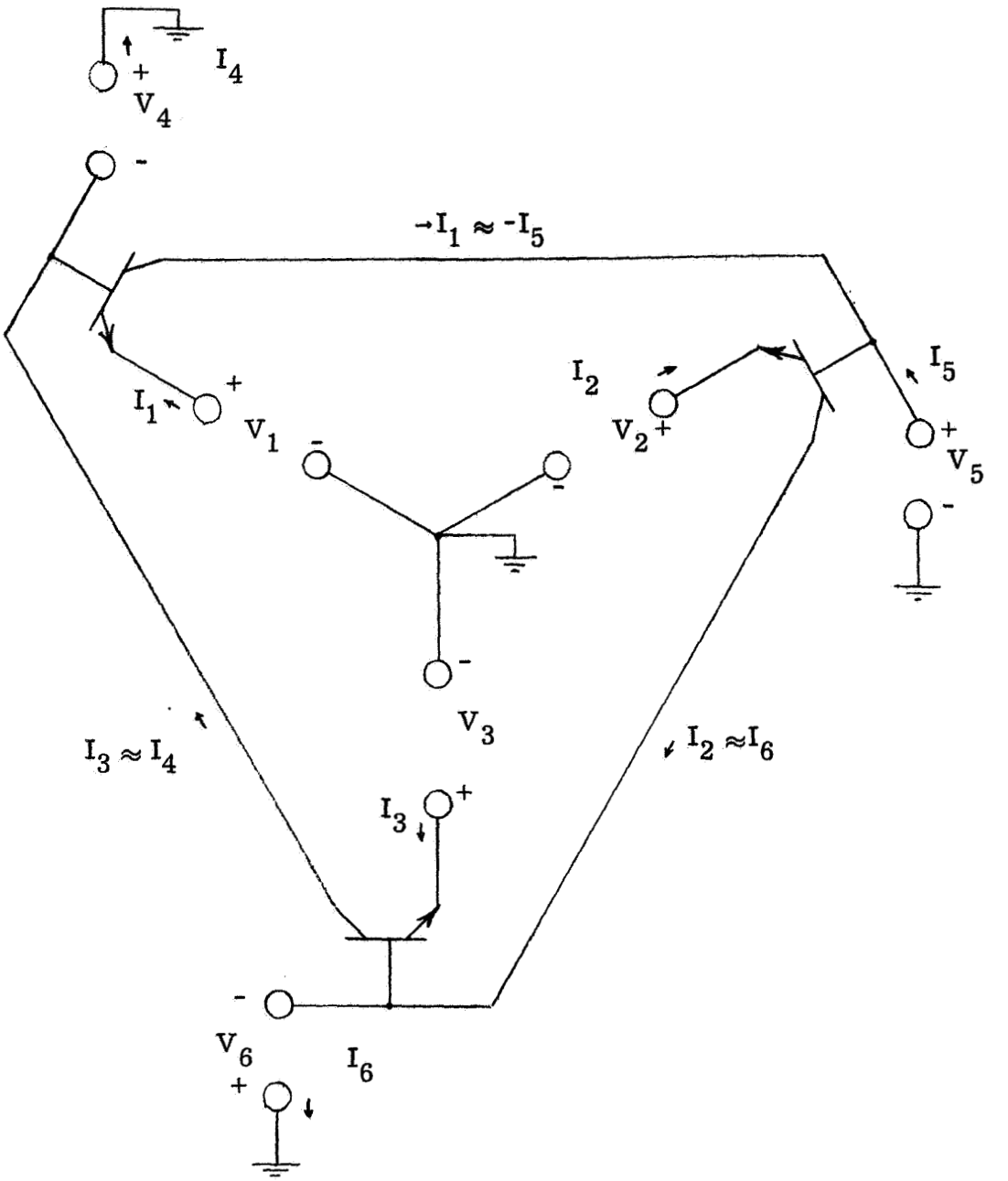

Figure 10. Six-Port Transistor Circuit

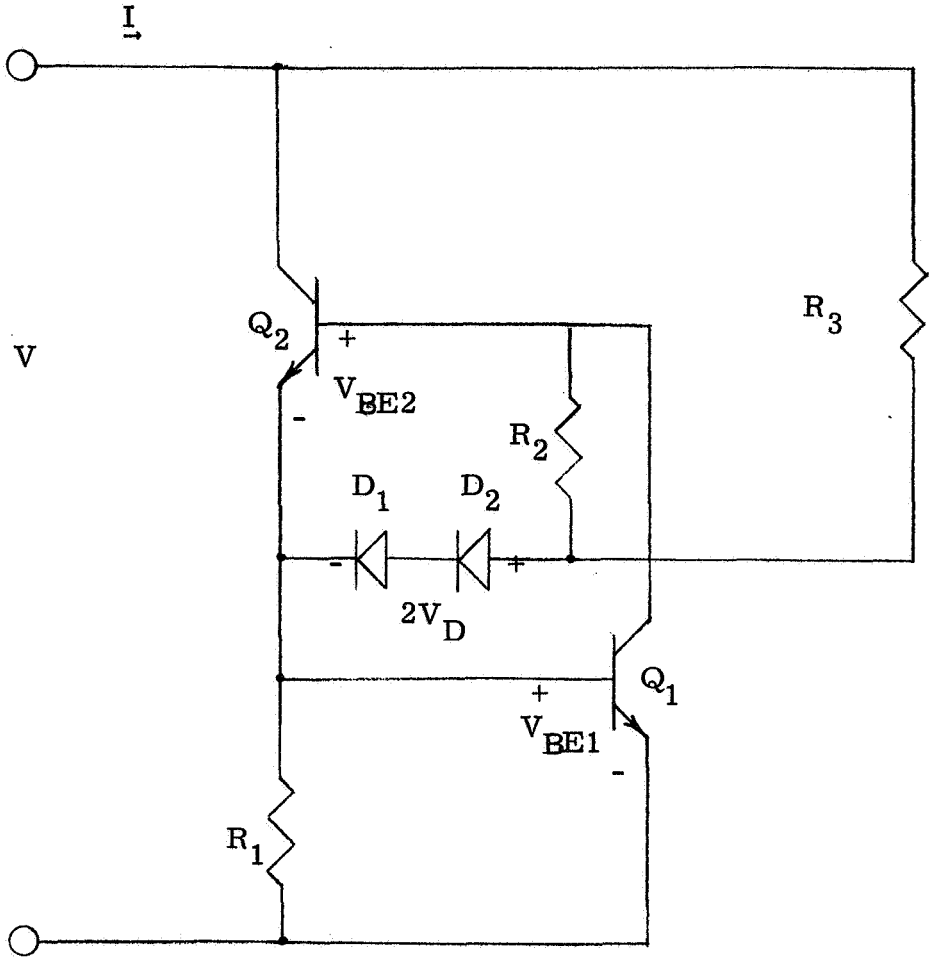

Figure 11. Two-Terminal Current Source

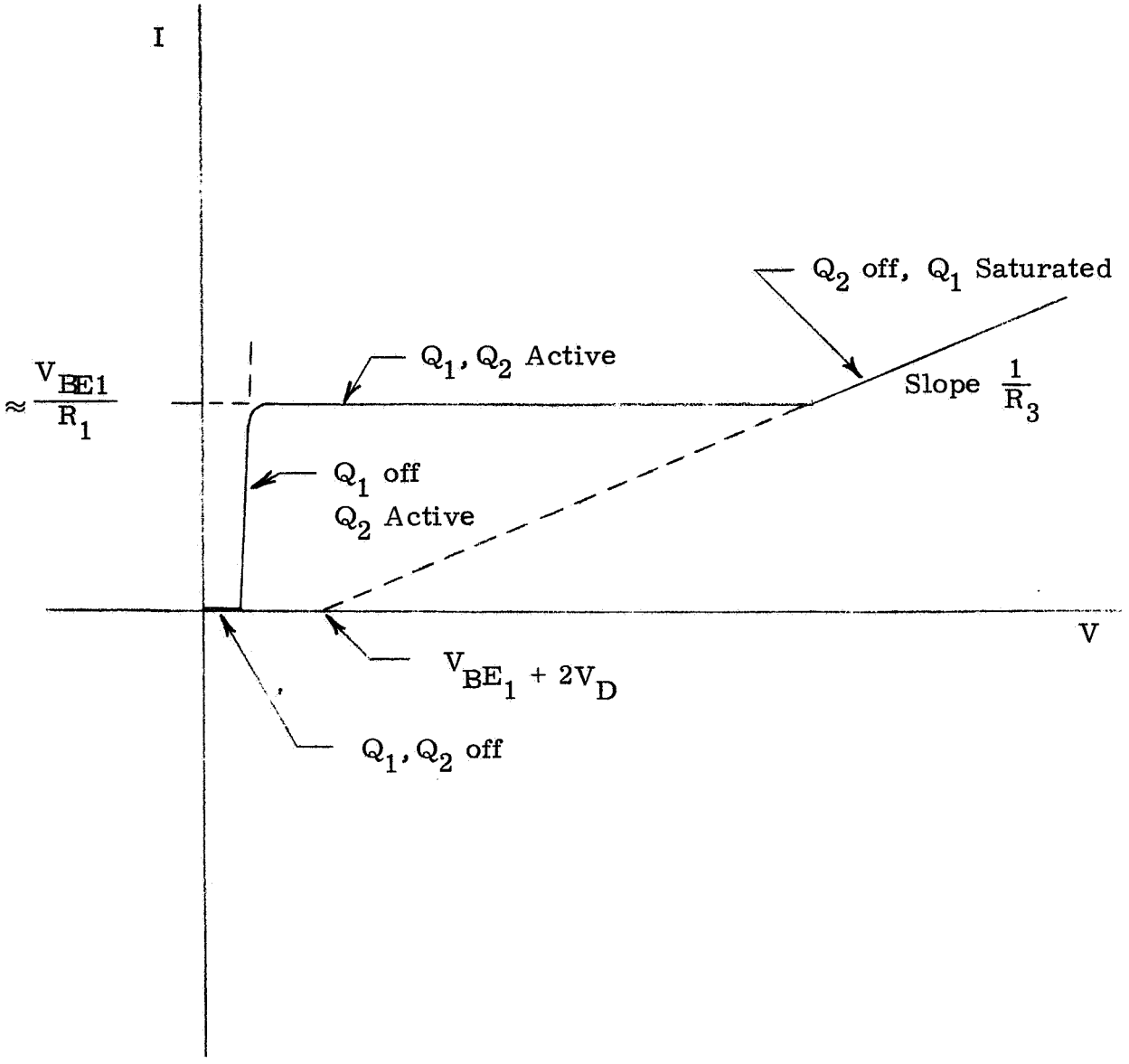

Figure 12. V-I Characteristic of Current Source

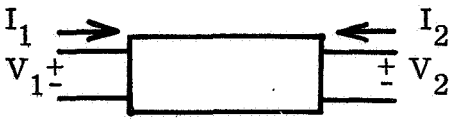

$$\begin{bmatrix} V_1 \\ I_1 \end{bmatrix} = \begin{bmatrix} \quad T \quad \end{bmatrix} \begin{bmatrix} V_2 \\ -I_2 \end{bmatrix}$$

P = Complex Frequency

Mutator	Inverting	Noninverting
L-R	$\begin{bmatrix} 0 & P \\ 1 & 0 \end{bmatrix}$	$\begin{bmatrix} P & 0 \\ 0 & 1 \end{bmatrix}$
C-R	$\begin{bmatrix} 0 & 1 \\ P & 0 \end{bmatrix}$	$\begin{bmatrix} 1 & 0 \\ 0 & P \end{bmatrix}$
L-C	$\begin{bmatrix} 0 & 1 \\ 1 & 0 \end{bmatrix}$	$\begin{bmatrix} P & 0 \\ 0 & \frac{1}{P} \end{bmatrix}$

Scalor	Current	Voltage	Power
	$\begin{bmatrix} 1 & 0 \\ 0 & K_I \end{bmatrix}$	$\begin{bmatrix} K_V & 0 \\ 0 & 1 \end{bmatrix}$	$\begin{bmatrix} K_V & 0 \\ 0 & K_I \end{bmatrix}$

Table 1. Transmission Matrices for Mutators and Scalors

Mutator	Type	Ports terminated in 1 ohm resistors	Ports terminated in 1 farad capacitors	Output Terminal
L-R	Noninverting	2, 4, 5	3	6
	Inverting	4, 5, 6	3	2
C-R	Noninverting	2, 3, 4	5	6
	Inverting	3, 4, 6	5	2
L-C	Noninverting	4, 5	2, 3	6
	Inverting	3, 4, 5, 6		2

Table 2. Terminations for Realizing Mutators

APPENDIX A

Stability of S-W Gyrator

An estimate of the capacitive loading required to stabilize the S-W gyrator may be obtained as follows. Suppose the gyrator of Figure 1 to be terminated with capacitance C_1 and C_2 at ports 1 and 2 respectively. Let the y parameters of the terminated gyrator be indicated with primes, thus:

$$\begin{aligned} y_{11'} &= y_{11} + C_1 s, \\ y_{22'} &= y_{22} + C_2 s, \\ y_{12'} &= y_{12} \\ y_{21'} &= y_{21}. \end{aligned} \tag{1A}$$

Substituting the expressions for the frequency dependence of transistor current gain as given in Figure 1 into Equations (1A) gives

$$\begin{aligned} y_{11'} &= \frac{\tau_1 s^2 + (1 + \tau_1 \omega_{\alpha 1})\, s + \omega_{\beta 1}}{R_1 (s + \omega_{\alpha 1})}, \\ y_{22'} &= \frac{\tau_2 s^2 + (1 + \tau_2 \omega_{\alpha 2})\, s + \omega_{\beta 2}}{R_2 (s + \omega_{\alpha 2})}, \\ y_{12'} &= \frac{\alpha_{02} \omega_{\alpha 2}}{R_2 (s + \omega_{\alpha 2})}, \\ y_{21'} &= \frac{-\alpha_{03} \omega_{\alpha 3}}{R_1 (s + \omega_{\alpha 3})}, \end{aligned} \tag{2A}$$

where $\tau_1 = R_1 C_1$, $\tau_2 = R_2 C_2$, and the subscripts on α_0, ω_α and ω_β refer to individual transistors as labeled in Figure 1.

For the gyrator to be stable it is necessary that the zeros of $y_{11}'y_{22}' - y_{12}'y_{21}'$ be in the left half plane. Upon substitution from Equation (2A), this reduces to the requirement that the zeros of a polynomial

$$P = As^5 + Bs^4 + Cs^3 + Ds^2 + Es + F$$

be in the left half plane (that P be a Hurwitz polynomial), where

$$\begin{aligned}
A &= \tau_1\tau_2, \\
B &= [\tau_1\tau_2\omega_{\alpha 3} + \tau_1(1 + \tau_2\omega_{\alpha 2}) + \tau_2(1 + \tau_1\omega_{\alpha 1})], \\
C &= [\tau_1(1 + \tau_2\omega_{\alpha 2})\,\omega_{\alpha 3} + \tau_2(1 + \tau_1\omega_{\alpha 1})\,\omega_{\alpha 3} \\
&\quad + (1 + \tau_1\omega_{\alpha 1})\,(1 + \tau_2\omega_{\alpha 2}) + \tau_2\omega_{\beta 1} + \tau_1\omega_{\beta 2}], \\
D &= [\tau_2\omega_{\beta 1}\omega_{\alpha 3} + \tau_1\omega_{\beta 2}\omega_{\alpha 3} + (1 + \tau_1\omega_{\alpha 1})\,(1 + \tau_2\omega_{\alpha 2})\,\omega_{\alpha 3} \\
&\quad + \omega_{\beta 1}(1 + \tau_1\omega_{\alpha 2}) + \omega_{\beta 2}(1 + \tau_1\omega_{\alpha 1})], \\
E &= [\omega_{\alpha 3}\omega_{\beta 1}(1 + \tau_2\omega_{\alpha 2}) + \omega_{\alpha 3}\omega_{\beta 2}(1 + \tau_1\omega_{\alpha 1}) + \omega_{\beta 1}\omega_{\beta 2} \\
&\quad + \alpha_{02}\alpha_{03}\omega_{\alpha 2}\omega_{\alpha 3}], \\
F &= [\alpha_{02}\alpha_{03}\omega_{\alpha 1}\omega_{\alpha 2}\omega_{\alpha 3} + \omega_{\beta 1}\omega_{\beta 2}\omega_{\alpha 3}].
\end{aligned} \tag{3A}$$

Equations (3A) may be simplified for present purposes by assuming that $\tau_1\omega_{\alpha 1} \gg 1$, $\tau_2\omega_{\alpha 2} \gg 1$, β_0 for all transistors is very much greater than one, and that the alpha cutoff frequencies are of the same order of magnitude.

$$A = \tau_1\tau_2,$$

$$B \approx \tau_1\tau_2(\omega_{\alpha 1} + \omega_{\alpha 2} + \omega_{\alpha 3}),$$

$$C \approx \tau_1\tau_2(\omega_{\alpha 1}\omega_{\alpha 2} + \omega_{\alpha 2}\omega_{\alpha 3} + \omega_{\alpha 1}\omega_{\alpha 3}),$$

$$D \approx \tau_1\tau_2\omega_{\alpha 1}\omega_{\alpha 2}\omega_{\alpha 3}, \tag{4A}$$

$$E \approx \omega_{\beta 1}\tau_2\omega_{\alpha 2}\omega_{\alpha 3} + \omega_{\beta 2}\tau_1\omega_{\alpha 1}\omega_{\alpha 3} + \omega_{\alpha 2}\omega_{\alpha 3},$$

$$F \approx \omega_{\alpha 1}\omega_{\alpha 2}\omega_{\alpha 3}.$$

Let

$$P(s) = M(s) + N(s), \tag{5A}$$

where

$$M(s) = Bs^4 + Ds^2 + F, \tag{6A}$$

and

$$N(s) = s(As^4 + Cs^2 + E). \tag{7A}$$

If P is to be Hurwitz, then M and N must have simple zeros on the $j\omega$ axis and the zeros of M and N must alternate.[8] The zeros of N are

$$s = 0; \quad s^2 = \frac{-C \pm C\sqrt{1 - \frac{4AE}{C^2}}}{2A} \tag{8A}$$

and the zeros of M are given by

$$s^2 = \frac{-D \pm D\sqrt{1 - \frac{4BF}{D^2}}}{2B}. \tag{9A}$$

If $4AE/C^2$ and $4BD/D^2$ are very much smaller than unity, as they are under the assumptions made, the zeros of N are

$$s = 0; \quad s \approx \pm j\sqrt{\frac{E}{C}}, \quad s \approx \pm j\sqrt{\frac{C}{A}} \tag{10A}$$

and the zeros of M are

$$s \approx \pm j\sqrt{\frac{F}{D}}; \quad s \approx \pm j\sqrt{\frac{D}{B}}. \tag{11A}$$

For the zeros of M and N to alternate:

$$CF < DE, \tag{12A}$$

$$BE < CD, \tag{13A}$$

$$AD < BC. \tag{14A}$$

Upon substituting Equations (4A) into the above, (13A) and (14A) are found to be satisfied under the assumptions made, and (12A) gives the answer sought:

$$\omega_{\beta 1}\tau_2\omega_{\alpha 2} + \omega_{\beta 2}\tau_1\omega_{\alpha 1} > \frac{\omega_{\alpha 1}\omega_{\alpha 2} + \omega_{\alpha 1}\omega_{\alpha 3}}{\omega_{\alpha 3}}. \tag{15A}$$

Section II

Metallurgical Studies of Microcircuit Interconnections

Welville B. Nowak

I. Introduction

A. Background

Thin, metallic films are used extensively in integrated circuits for electrodes, for interconnections paths, and for supporting (beam) leads. In many cases aluminum may be successfully used. In other cases, however, aluminum presents difficulties, and recourse must be had to multilayers of different metals in order to meet a complex set of requirements.

One of the failure modes of microcircuits subjected to storage, processing, or operating "stresses" is deterioration of the interconnection paths. This has been observed[1,2] for aluminum metalization on SiO_2 held at 450°C for 30 minutes (or longer times at lower temperatures) or at current densities above 10^6 amps/cm^2. Manifestations of this deterioration are:

1. increased electrical resistance of the interconnections,
2. open interconnections (total "disappearance" of metalization),
3. ragged edges of the paths,
4. loss of adhesion between interconnection and substrate.

Mechanisms leading to this deterioration include diffusion, chemical reaction, and electromigration.

To reduce this type of failure, composite systems have been tried and analyzed.[1,2,3,4] Of these various systems, gold-molybdenum (Au-Mo) is typical of those with promise. The molybdenum forms a good bond to the substrate and the gold overlayer adheres well to the molybdenum and provides

a low resistance interconnection. The good bond between molybdenum and substrate is provided by the chemical affinity of molybdenum to oxygen and to silicon. On metallurgical grounds this system is expected to result in relatively few failures (and this appears to be the case in practice) because[5,6]:

1. there are no intermediate phases,
2. the eutectic temperature is high (1054°C),
3. the solubility of Au in solid Mo is exceedingly small,
4. the solubility of Mo in Au is small, about 1 atomic percent.

However, even this system can deteriorate in certain cases[2], and it would seem that a closer look is needed into thin film interactions as opposed to those between bulk materials (with which most literature data has been obtained).

It is well known that diffusion and many chemical reactions may proceed far faster in thin films than in bulk material, presumably because of greater density of defects in films. This knowledge is often of a qualitative nature for two reasons: (1) the character of films varies widely with their fabrication processes, and (2) analysis of the interactions is difficult. There is a need to measure interactions and their rates between thin films and between films and subtrates as a function of film character and as a function of interaction time and temperature in appropriate environments (such as air, nitrogen, water vapor, and/or radiation flux). These measurements are needed for understanding observed phenomena, for predicting failure modes in a given environment, and for taking logical steps to reduce failures by changes in materials, design, or processing.

B. Objective of Program

The objective of this program is to measure quantitatively the interdiffusion between certain metallic films. Emphasis will be placed on laminated films and on substrates of practical importance. Techniques

will be developed for obtaining interdiffusion profiles, if possible. The purpose for undertaking this program is not only to fill gaps in our technical knowledge of thin film behavior, but to lead directly to improvements in the realiability and predictability of integrated circuits of particular importance to NASA.

C. Approach

The difficulties in obtaining diffusion (concentration) profiles in thin films reside in (1) the chemical analysis of very thin, sectioned layers and (2) the removal and thickness determination of these very thin layers.

A perusal of modern techniques has led us to the conclusion that composition analysis by means of optical spectral-reflectivity has the greatest potential for success in overcoming the first class of difficulties. The second class of difficulties is circumvented either by lapping the specimen at a small angle and analyzing at high optical magnification, or by removal of thin sections chemically (or via sputtering) with section thickness determined interferometrically or with an air-gage.

Figure 1 is a schematic illustration of a bi-metal conductor system on SiO_2 on a Si substrate. Also shown in the Figure is the position of a small-angle lapping cut. In practice, such a cut would be made at an angle of several degrees with the surface and would thus expose material below the surface at a lateral magnification.

If such a cut were examined by spectral reflectivity under a microscope, a measure of the concentration profile might be obtained. Since the penetration depth of visible light into metals of interest is 40-70 Å, the reflectivity would characterize virtually the surface composition.

The films are to be evaporated as strips on glass microscope slides and on oxidized Si wafers. Deposition parameters to be controlled include: film thickness (about 5000 Å, deposition rate (50 to 300 Å/min), and substrate temperature (about 200°C). Commercial, oil-pumped, liquid-N_2 trapped vacuum evaporators are to be used, with pressures between 10^{-6}

and 10^{-5} torr. The films will be characterized as far as possible in the following ways:

1. residual stresses,
2. electrical resistivity (near 300°K and 77°K),
3. temperature coefficient of resistivity (near 300°K),
4. crystallite (or grain) size.

This characterization will be attempted after the techniques have been developed for obtaining the diffusion data.

II. Summary of Results

A. Literature Survey

At the start of this program it was known that there was scant literature available on diffusion in thin films, and it was thought that the optical reflectivity approach was novel. A literature search revealed less than a dozen papers concerning thin film diffusion, but also revealed that Schopper[7] used optical reflectivity for observing this phenomenon. The most extensive and definitive work has been carried out by Weaver and Hill[8] and Weaver and Brown[9,10,11] in Scotland utilizing an optical reflectivity method. These authors did not obtain concentration profiles, but inferred an error function behavior by observing overall distance/(time)$^{1/2}$ dependence. In certain cases they noted very rapid initial diffusion. They were able to verify that the activation energies and diffusion constants for their films were comparable to bulk material in most cases. In silver-aluminum films less than 2000 Å thick, the diffusion constant increased as film thickness decreased going from a value of 2.7×10^{-14} cm^2/sec to 1.9×10^{-13} cm^2/sec for a film 60 Å thick.

Since our program will attempt to utilize spectral reflectivity as a function of wavelength over the visible spectrum (in contrast to most previous investigators who selected one "most sensitive" wavelength) as an indicator of chemical composition, a literature search was started for spectral reflectivity of elements and alloys.

Figure 2 illustrates the spectral reflectivity of several metals as a function of wavelength, derived from literature values. It is the variation of the spectral reflectivity with composition that is important in this program, but data for this are very scarce. Figures 3 and 4, for the systems Ag-Al and Au-Pd, respectively are the only data found thus far.

Optical Equipment

Inasmuch as a grating monochromator was not available for the spectral reflectivity measurements, an attempt was made to utilize a prism spectrometer. This instrument has a built-in collimator, telescope and slit. It has been calibrated with a helium discharge tube. In operation, a tungsten iodide light source is used. The output of the spectrometer is directed into the side-illumination aperature of a metallurgical microscope.

The light output is detected at the microscope eyepiece with either a CdS photodetector or a Si solar cell. The short circuit current of the latter has proven more stable and convenient to measure than the CdS resistance change.

However, it was found that the spectrometer slit width (and resultant wavelength pass-band) versus intensity of transmitted light was not readily optimized. Mechanical stability problems also arose. Therefore, this equipment has been set aside and a set of moderately narrow-band color filters procured. Although the pass-bands and transmittance of these filters are not as good as dielectric film filters, their cost is much less and they are adequate for our purpose.

The set of filters comprise the following (for incandescent light):

Filter	Dominant Wavelength (Å)
Wratten 70	6780
Wratten 72B	6060
Wratten 73	5760
Wratten 74	5380
Wratten 75	4900
Corning Red	6330

C. Sectioning Techniques

1. Angle-Lapping

Considerable effort has been expended in attempting to develop an angle lapping method for thin metallic films on oxidized silicon. No success has been achieved. In every case the films were severely distorted.

Al on SiO_2 on Si was examined using standard semiconductor angle-lapping techniques and an alumina-water slurry on glass. Poor adherence of the films was noted except for very thin translucent films. These thin Al films were probably converted to Al_2O_3 during the lapping. The use of non-aqueous slurries did not improve matters, and investigation of this system was discontinued.

A Zn-Ni multilayer system was investigated as a possible stand-in for Au-Mo. During the lapping, poor adherence was found between Ni and SiO_2 and between Zn and Ni, and this system was abandoned.

Pt on Cr on SiO_2 on Si yielded some better adherence than the above systems, especially with non-aqueous slurries. However, the fundamental problem appeared to be flow and smearing of the films.

A standard metallographic technique for sectioning thin films is to prepare a sandwich by adding a covering layer onto the film. Various attempts were made to accomplish this with the Pt-Cr system. Plastics and electroplated Ni were used with no success. More elaborate sandwiches were prepared by bonding Si slices to Cr-Pt-Cr-SiO_2-Si specimens with low melting metals such as Sn and In. The most successful combination utilized In. At 80X the region containing the metallic films was well defined, but the individual layers were not. Chemical etching did not seem to resolve the difficulties.

Consequently, work on the angle-lapping technique was stopped, although the technique would have high utility were it to be successful.

2. Sputter-Etching

Work has been started on the determination of the parameters for removal of thin layers by sputtering. Certain instabilities in the gas discharge have

been observed that lead to uneven removal over the specimen area. Corrective action is being taken via electrode redesign and substitution of a more stable power supply.

Possible difficulties with this technique are over-heating of the films despite attachment of sample to a water cooled heat sink, and direct disturbance of the diffusion profile by the ion bombardment. The first effect can be directly evaluated by thermocouples. The latter effect may be more difficult to assess.

III. Conclusions

The use of optical reflectivity techniques, together with sputter-removal of thin layers may be a viable method for determination of concentration profiles in thin film interdiffusion. However, optical reflectivity technique applied only to the surface of the films can still yield diffusion constant and activation energy values that are important in assessing reliability of thin films as used in microcircuits.

IV. REFERENCES

1. W. M. Berger, R. S. Keen, G. L. Schnable in "Physics of Failure in Electronics," Vol. 4, 1966, Report No. 637529, Defense Documentation Center, Alexandria, Virginia 22314.
2. "Advanced Technology of Interconnections in Microelectronics," May, 1967, Interim Scientific Report prepared by Motorola, Inc. for the National Aeronautics and Space Administration, Electronics Research Center, Cambridge, Massachusetts under Contract No. NAS 12-132.
3. W. H. Gianelle in "Physics of Failure in Electronics," Vol. 4, 1966, Defense Documentation Center Report No. 637529.
4. J. A. Cunningham, Solid State Electronics, 8, 735 (1965).
5. M. Hansen, Constitution of Binary Alloys, McGraw-Hill Book Company, New York, 1958.
6. G. A. Geach and D. Summers-Smith, Journal of the Institute of Metals, 82, 471 (1953 - 1954).
7. H. Schopper, Zeit, f. Phys., 143, 93 (1955).
8. C. Weaver and R. M. Hill, Advances in Physics, 8, 375 (1959).
9. C. Weaver and L. C. Brown, Phil, Mag., 7, 1 (1962).
10. C. Weaver and L. C. Brown, Phil. Mag., 8, 1379 (1963).
11. C. Weaver and L. C. Brown, Phil. Mag., 17, 881 (1968)
12. H. Rohl, Ann. d. Phys., 18, 155 (1933).

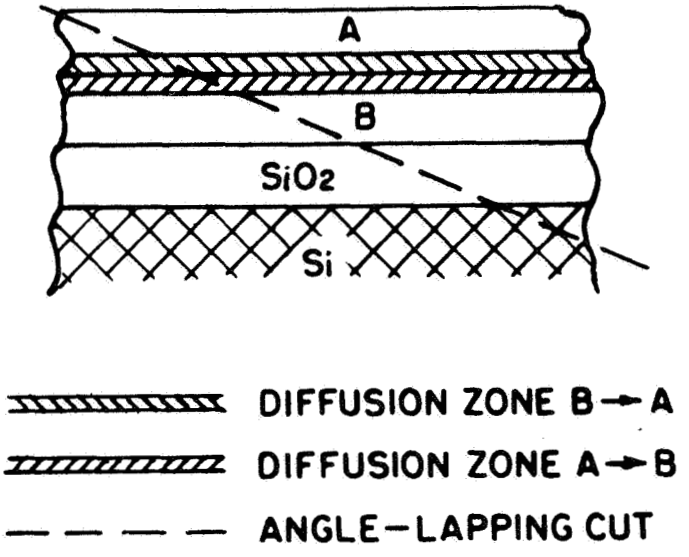

Figure 1. Schematic drawing of angle-lapping cut through interduffused bi-metal laminated film.

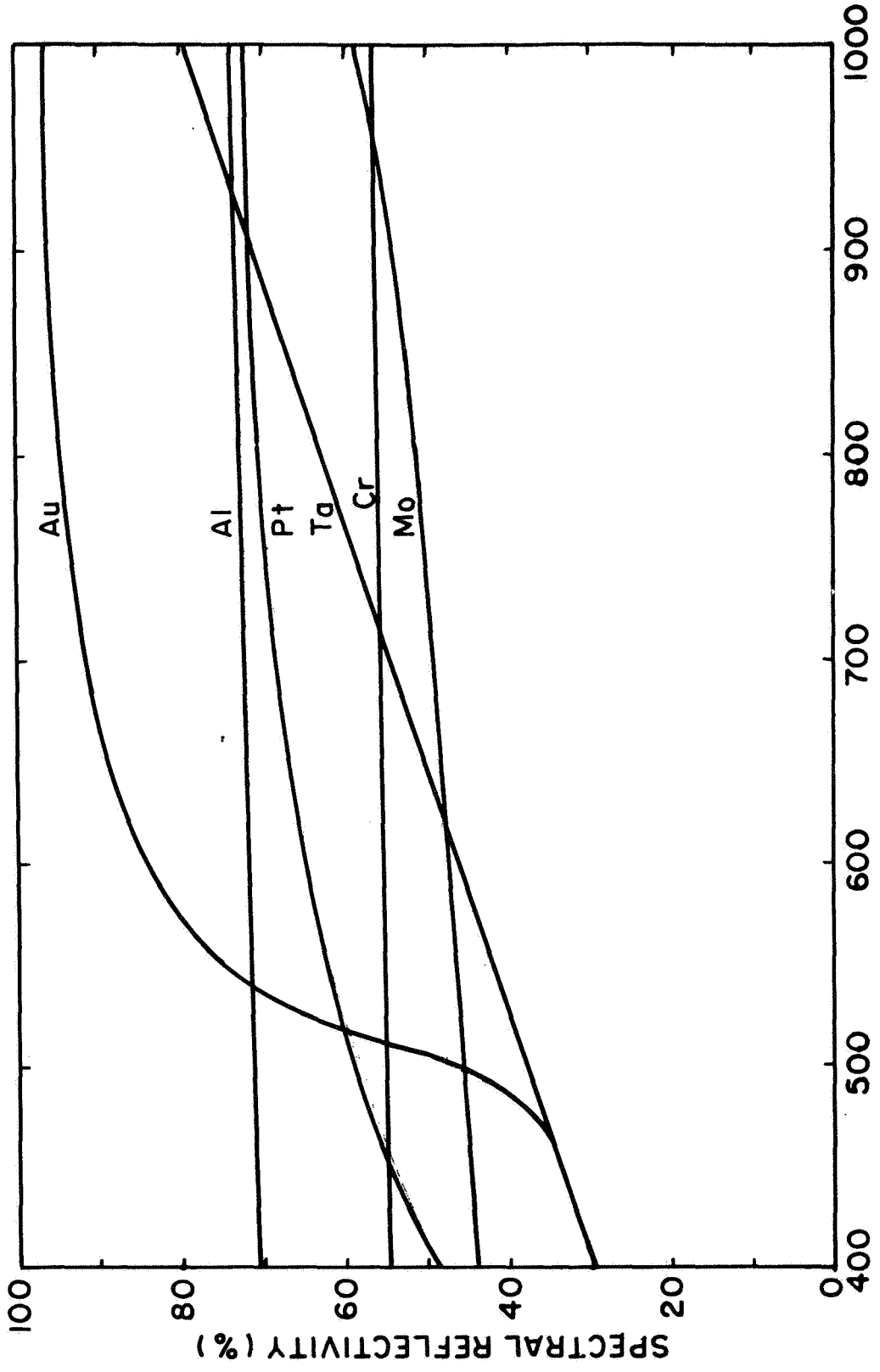

Figure 2. Spectral reflectivity of several metals (derived from the literature).

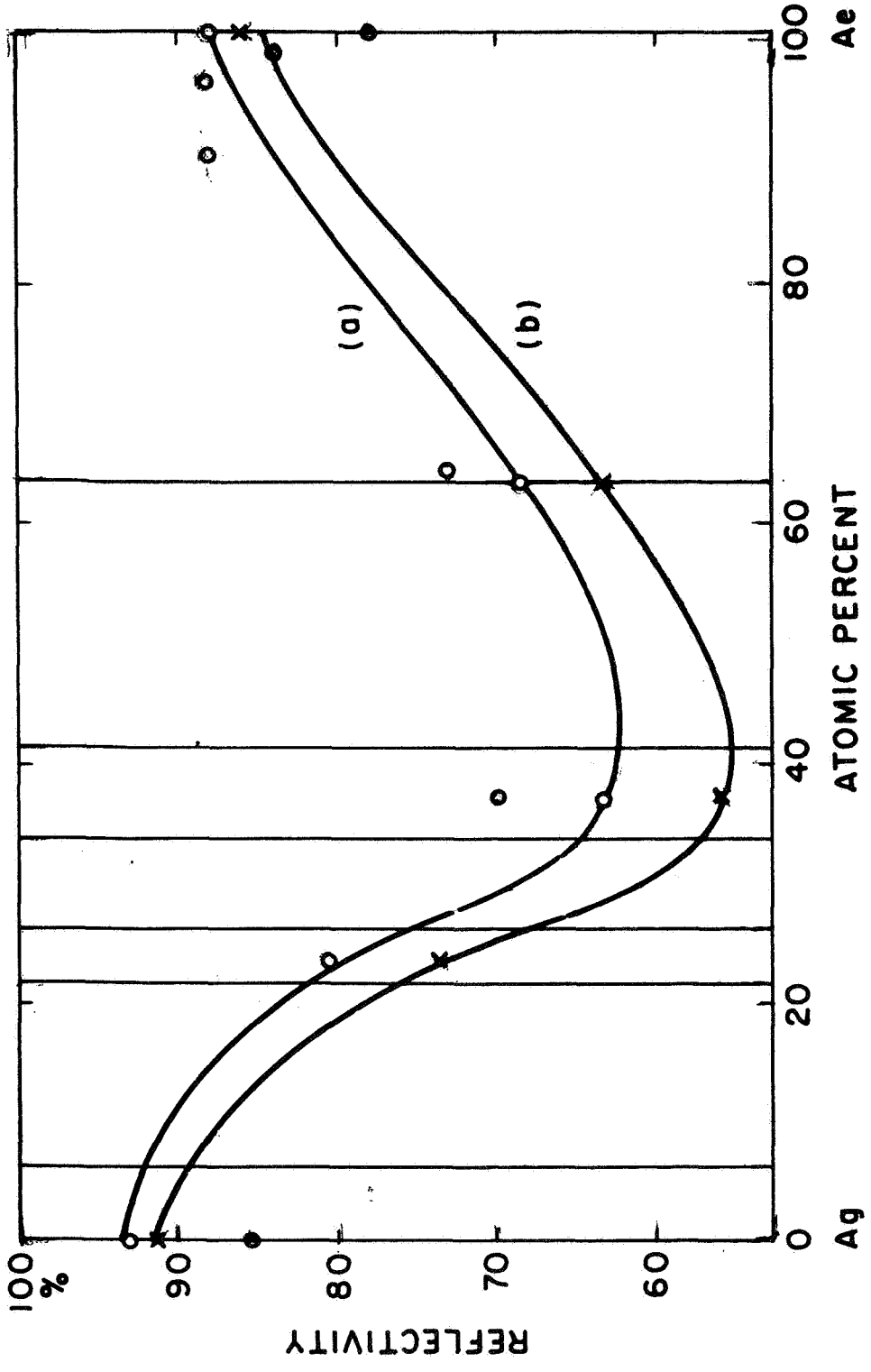

Figure 3 Spectral reflectivity of Ag-Al alloys (Weaver and Brown, Ref. 11).

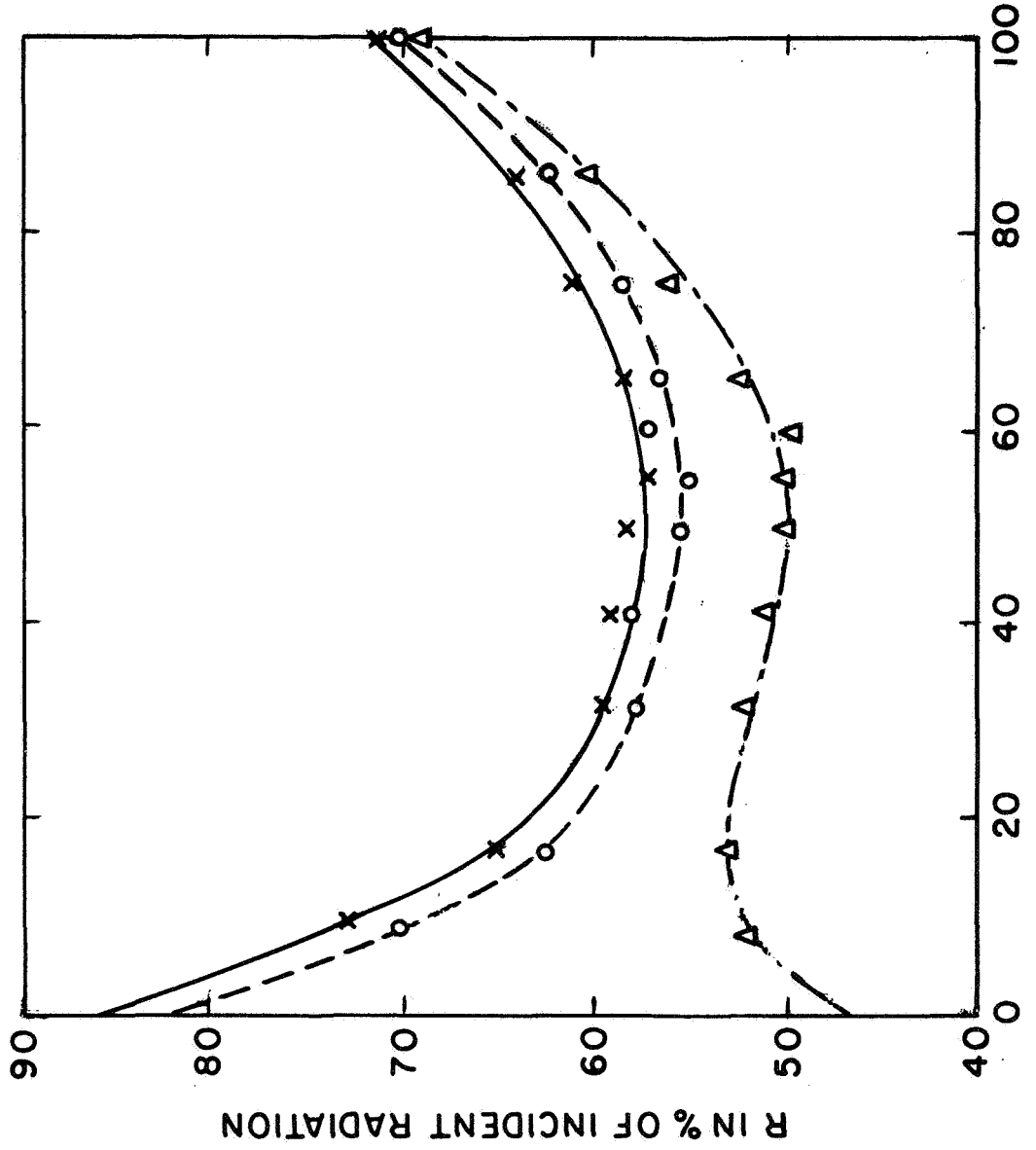

Figure 4 Spectral reflectivity of Au-Pd alloys (Rohl, Ref. 12).

Section III

Biophysical Studies

S. Fine

The National Aeronautics and Space Administration is involved in a number of projects which require the use of lasers at a number of wavelengths, power and energy levels. In many of these studies it is necessary to know the thresholds for injury at the laser wavelength used in order that adequate precautions can be taken to minimize the hazard. Thus the operational capabilities of the laser system can be optimized. Furthermore, with the increasing use of lasers, information regarding the effects of threshold and suprathreshold radiation, on both a short and long term basis, is important to the civilian populace in order to permit assessment of the degree of injury and to allow consideration to be given to meaningful methods of therapy, should accidental injury occur.

Another area of interest to the National Aeronautics and Space Administration is the application of knowledge and understanding gained through in-house research and through extramural grants and contracts to areas of biology and medicine, so as to improve medical care both on a national and on an international basis.

Consequently, some of the effort supported in part by this contract during this past period have been devoted to assessing and delineating some of the hazards associated with laser radiation of specific characteristics and determining methods in which laser radiation can be used as a tool in biology and medicine. The results obtained will be of value to the country as a whole with regard to delineation and minimization of laser hazards and to medicine and biology where lasers are used as a tool.

The following is, therefore, an outline of the laser related areas which have been supported in part by this contract.

1. "Toxic and Explosive Hazards Associated with Lasers," D. MacKeen, S. Fine, and E. Klein, published in Laser Focus, pp. 47-49, October 1968.

In this publication, consideration is given to hazards associated with ancillary materials as well as with the active laser media. These could be encountered either during manufacture of the equipment or during its use. Elements and compounds presently used whether in the manufacture of the equipment or in conjunction with their operation were divided into six groups. The scope of each group extended from the relatively innocuous to the extremely hazardous. The value of this report is that it should alert the industry, including NASA contractors, to potential chemical and toxic hazards which may arise. Some safety procedures which can be initiated are recommended.

2. "Application of Thermal Models to Retinal Threshold Injury," W. P. Hansen and S. Fine, presented at the Laser Industry Association Meeting, October 24-26, Washington, D. C., to be published in Proceedings.

Helium neon lasers are in common use at NASA as well as throughout the country. In this report, analytical techniques were described for estimating the maximal retinal temperature elevation occurring during a step input of laser power to a retinal image of given size. It was shown that for a 10 micron retinal image diameter, the maximum temperature elevation cannot be limited by a voluntary avoidance reaction on the part of the observer. Thus, the hazards involved in the use of He-Ne (and similar) lasers has been more clearly delineated then previously. This is of interest to NASA, its contractors and to the civilian populace as a whole.

3. "Exploration of Potential Carcinogenic Effects of Pulsed Laser Radiation," F. Bock, Y. Laor, S. Fine, and E. Klein, presented at the Laser Industry Association meeting, October 24-26, Washington, D. C., to be published in Proceedings.

There is a greater propensity for malignant transformation following burns of the skin. Since pulsed laser radiation as produced with ruby

lasers produces a burn as well as possibly other effects, investigations of the potential for production of cancer following ruby laser radiation is of significance. Long term studies of the tendency for malignant transformation following pulsed laser irradiation with and without a co-carginogen were consequently carried out on mice. The results to date have not shown any significant increase in the rate of tumor formation following pulsed ruby laser irradiation. It should, however, be understood that extrapolation of this data to man is, of course, difficult since as is well known there are species differences for malignant transformations. The studies should, however, at least provide some guidelines for follow up in the case of accidental injury or where lasers are employed as a therapeutic modality.

4. "Anterior Chamber Measurements on CO_2 Laser Corneal Irradiation," S. Fine, D. MacKeen, L. Feigen, and B. S. Fine, published in Proceedings of the Annual Conference on Engineering in Medicine and Biology, Vol. 10, November 1968.

Previous studies have shown that anterior identation of the lens occurs on fixation in gluteraldehyde following suprathreshold rabbit corneal irradiation, without perforation of the cornea. In this report, the mechanism by which the lens alteration occurs was examined. It was shown that increased pressures and temperatures are produced in the anterior aqueous chamber. Above a certain temperature-pressure level, alterations in the lens of the eye could be produced which on fixation resulted in indentation. Below this level, indentation did not occur. Coincident with the changes in the anterior chamber, flattening of the cornea occurred, thus bringing this "secondary heat source" into closer approximation to the lens. These alterations in the lens are of significance since they may affect the therapeutic procedures considered.

5. "Corneal Calcification," B. S. Fine, J. Berkow, and S. Fine, Science, Vol. 162, October 4, 1968, pp. 129-130.

In studies on the effects of continuous CO_2 laser irradiation of the cornea, a number of rabbit eyes developed clinical and histopathological

changes identical with band keratopathy as observed in the human cornea. The calcification was entirely extracellular and characterized as hydroxyapatite by x-ray diffraction. The lesions, examined by electron microscopy, appeared as calcific spherules and conglomerates. The extracellular form of calcification obtained differed in morphologic features from the intracellular calcification that has been seen in hyperparathyroidism, but was similar to band keratopathy on humans.

The National Aeronautics and Space Administration is concerned with the properties and capabilities of biological systems, in particular human systems, since these will affect man's ability to successfully undertake prolonged extraterrestial travel. Medicine is also concerned with the properties and capabilities of human systems. In some cases, various tissues are used as allografts, homografts or heterografts. Methods for sterilization and preservation of biological tissue are of importance to NASA and to medicine. Consequently, some attention has been directed to the area of investigation discussed below.

6. "Rupture and Tensile Strength Measurements of Fresh and Treated Canine Aortic Tissue," S. B. Litwin, J. Cohen, S. Fine, and A. Aaron, Proceedings of the Annual Conference on Engineering in Medicine and Biology, Vol. 10, November 1968.

Successive transverse sections of normal and treated canine aortas were cut to a standard size from the ascending aorta to the common iliac vessels. The aortas were sterilized with beta-propiolactone, or stored either in a graft bank at -70°C for 3 to 30 days or in a 4% buffered formaldehyde mixture for 1 to 19 days. Using an Instron test machine, specimen thickness, force-elongation curves, the maximum force for rupture and the tensile strength were obtained. The variation of rupture strength and tensile strength with position along the untreated aorta were determined and the effect of the treatment on rupture force and tensile strength assessed.